Geochronology and Genetic Model for Early Cretaceous Volcanic Rocks from the Southern Qiangtang Terrane, Northern Tibet, China: Constraints from U-Pb Zircon Dating, Whole-Rock Geochemical and Sr-Nd Isotopic Data

LIU Shen[1,*], FENG Caixia[1], M. Santosh[1,2,3], FENG Guangying[4], XU Mengjing[1], Ian M. COULSON[5], GUO Xiaolei[1], GUO Zhuang[1] and FAN Yan[1]

1 *State Key Laboratory of Continental Dynamics and Department of Geology, Northwest University, Xi'an 710069, China*

2 *China University of Geosciences Beijing 100083, Beijing, China*

3 *Department of Earth Sciences, University of Adelaide, Adelaide SA 5005, Australia*

4 *Institute of Geology, Chinese Academy of Geological Sciences, 100037 Beijing, China*

5 *Solid Earth Studies Laboratory, Department of Geology, University of Regina, Regina, Saskatchewan S4S 0A2, Canada*

Abstract: Post-collisional volcanic rocks of Mesozoic age occur in the regions adjacent to Gerze, part of the southern Qiangtang Terrane of northern Tibet, China. Geochronological, geochemical, and whole-rock Sr-Nd isotopic analyses were performed on the volcanic rocks to better characterize their emplacement age and models for their origin. Laser ablation-inductively coupled plasma-mass spectrometry (LA-ICP-MS) U-Pb zircon analyses yielded consistent ages ranging from 123.1±0.94 Ma to 124.5±0.89 Ma for six volcanic rocks from the study area. The intermediate volcanic rocks belong to the alkaline and sub-alkaline magma series in terms of K_2O+Na_2O contents (5.9%–9.0%), and to the shoshonitic and calc-alkaline series on the basis of their high K_2O contents (1.4%–3.3%). The Gerze volcanic rocks are characterized by the enrichment of light rare earth elements [$(La/Yb)_N$=34.9–49.5] and large–ion lithophile elements (e.g., Rb, Ba, Th, U, K, Pb, and Sr), slightly negative Eu anomalies (Eu/Eu*=0.19–0.24), and negative anomalies in high field strength elements (e.g., Nb, Ta, Hf and Ti), relative to primitive mantle. The samples show slightly elevated $(^{87}Sr/^{86}Sr)_i$ values that range from 0.7049 to 0.7057, and low $\varepsilon_{Nd}(t)$ values from −0.89 to −2.89. These results suggest that the volcanic rocks studied derived from a compositionally heterogeneous mantle source and that their parent magmas were basaltic. The more mafic, parental magmas to the Gerze volcanic rocks likely underwent fractional crystallization of clinopyroxene, hornblende, biotite, and potassium feldspar, during ascent, with little to no crustal contamination, prior to their eruption/emplacement. While these volcanic rocks exhibit geochemical signatures typical of magmas formed in a destructive plate-margin setting, it is plausible that their mantle source might also have acquired such characteristics in an earlier episode of subduction.

Key words: volcanic rock, U–Pb age–dating, origin, Qiangtang Terrane, northern Tibet

1 Introduction

As the product of north to south collisional tectonics, the Qinghai–Tibet orogenic belt comprises the Songpan–Ganzi, western Qiangtang, eastern Qiangtang, and Lhasa terranes, respectively, by a series of sutures: the Jinshajiang, the Bangongco-Nujiang, the Hongjishan–Gemuri-Shuanghu, and the Yarlung Zangbo sutures (Allègre et al., 1984; Chang et al., 1986; Dewey et al., 1988; Pearce and Deng, 1988; Bureau of Geology and mineral resources of Tibet Autonomous Region, 1993; Yin and Harrison, 2000; Wang Yang, 2007; Zhang et al.,

* Corresponding author. E-mail: liushen@vip.gyig.ac.cn; liushen@nwu.edu.cn

2006a, b). The Songpan-Ganzi Terrane hosts Triassic abyssal flysch complexes, many thousands of meters in thickness. There is some debate, however, concerning the sedimentary origin of these rocks (Wang Yang, 2007). The youngest formation within this sequence includes Norian–Rhaetian aged strata; some boulders of limestone and basalt have also been found in this Terrane (Sichuan Bureau of Geology and mineral resources, 1991). Presently, there is intense controversy concerning the nature of the basement to the Songpan–Ganzi Terrane.

The Qiangtang and Lhasa Terranes are the main components of the Qinghan–Tibet plateau (Girardeau et al., 1984, 1985; Dewey et al., 1988; Yin and Harrison, 2000). In general, the Qiangtang Terrane can be divided into western and an eastern Terranes (Li Cai et al., 1995; Zhang et al., 2006a). A large number of ancient metamorphic rocks have been identified in the central region of the Qiangtang Terrane. It is unclear, however, as to whether these rocks, dated at 1.65±0.36 Ga (Zhang et al., 2007), represent the crystalline basement to this Terrane. Late Paleozoic strata occur in the area adjacent to Longmucuo (BGMRTAR, 1993; Kapp et al., 2003). Triassic strata mainly occur along the southern margin of aforementioned Paleozoic strata (BGMRTAR, 1993). Jurassic lithologies mainly comprise intermediate–felsic volcanic rocks, including pyroclastic units, and, locally, some limestone and siltstone (BGMRTAR, 1993). In addition, some early Cretaceous marine carbonates also occur.

Lhasa Terrane is located between the Bangongco–Nujiang Suture zone and the Brahmaputra Suture zone (Dewey et al., 1988; Yin and Harrison, 2000). This terrane comprises both Mesozoic sedimentary strata and the products of calc-alkaline volcanism (Burg et al., 1984; England and Searle, 1986; Dewey et al., 1988; Yin and Harrison, 2000). The strata in these two regions include gneiss, granite–gneiss, melange, marble, metamorphosed sedimentary rocks, and quartz sandstone (BGMRTAR, 1993). Gneiss from these areas has been demonstrated to have experienced tectonism, related to pan–African and a younger episode of metamorphism (Xu et al., 1985; Guynn et al., 2006). Strata of Ordovician to Permian age appear in the central region of Lhasa Terrane (Leeder et al., 1988; Yin et al., 1988). Jurassic strata are mainly distributed in the north and northeast parts of Lhasa Terrane (Leeder et al., 1988; BGMRTAR, 1993). Cretaceous strata are widely distributed across northern Lhasa Terrane.

The sutures in Qinghai–Tibet represent an evolutionary history related to extension, subduction and final collisional closure of oceanic crust. In general, the ophiolite within the Jinshajiang Suture mainly occurs in southeastern Jinshajiang, and is thought to have formed in the Triassic (Pearce and Deng, 1988; Wang Yang, 2007). At present, the nature of the Hongji mountain–Gemuri–Shuanghu Suture (Dewey et al., 1988) and any evidence for extensional tectonics in the development of this suture is limited. This suture exhibits a fault evolutionary history of continental crust (Li Cai et al., 2001), as well as the denudation of gneiss in the southern Qiangtang Terrane (360–350 Ma; Kapp et al., 2003). The opening of an ocean and the formation of new oceanic crust in this region occurred during the late Carboniferous–early Permian (Kapp et al., 2003); Late Permian to mid Triassic times marked an important change, to collisional tectonics and subduction of the oceanic crust (Dewey et al., 1988; Pearce and Deng, 1988; Yin and Harrision, 2000; Kapp et al., 2003). The Yarlung Zangbo Suture records the evolutionary history of the new Tethys Ocean between the Asia and the Indian continents (Dewey et al., 1988; Yin and Harrision, 2000; Lai et al., 2018). Based upon earlier studies, the opening of the new Tethys Ocean occurred between the late Triassic and early Jurassic (Yin and Harrision, 2000), and the closure time of this oceanic crust, mainly occurred during the Eocene (Rowley, 1996).

Mesozoic volcanic rocks are widespread in the northern Qinghai–Tibet belt; and investigation of these rocks can provide important information for understanding the history of volcanism and tectonism in this part of Asia. Earlier studies of the Mesozoic volcanic rocks of the Qinghai–Tibet belt focused on the rocks that post–date the collision between the Indian and Asia continents (Deng Wanming, 1989, 1998, 1999; Turner et al., 1996; Ding et al., 1999, 2003, 2007; Miller et al., 1999; Lai Shaocong and Liu Chiyang, 2001; Liu Shen et al., 2003; Liu et al., 2008; Williams et al., 2004; Chi Xiaoguo et al., 2005; Chung et al., 2005; Guo et al., 2006; Li Cai et al., 2006; Zhou Hua et al., 2016; Fig. 1a–b). By contrast, few studies have focused on the Mesozoic volcanic rocks in the Gerze region of the Qiangtang Terrane. To this background, and with an aim to better characterise this important episode of collisional tectonics and associated magmatism, in Asia during the Mesozoic, we present herein the results of our studies of representative volcanic rocks from the Nile, Yaduo, Quegang, and Xiuba, Gerze counties and regions of the southern Qiangtang Terrane. Our data include: new zircon U-Pb age data, determined by LA-ICP-MS, whole-rock major and trace element geochemistry, and whole rock Sr-Nd isotopic data. We use this comprehensive dataset to constrain the emplacement age(s), and present a model for the origin of the Mesozoic volcanic rocks in the study area.

2 Geological Setting

As the border region of western China, the Gerze area is

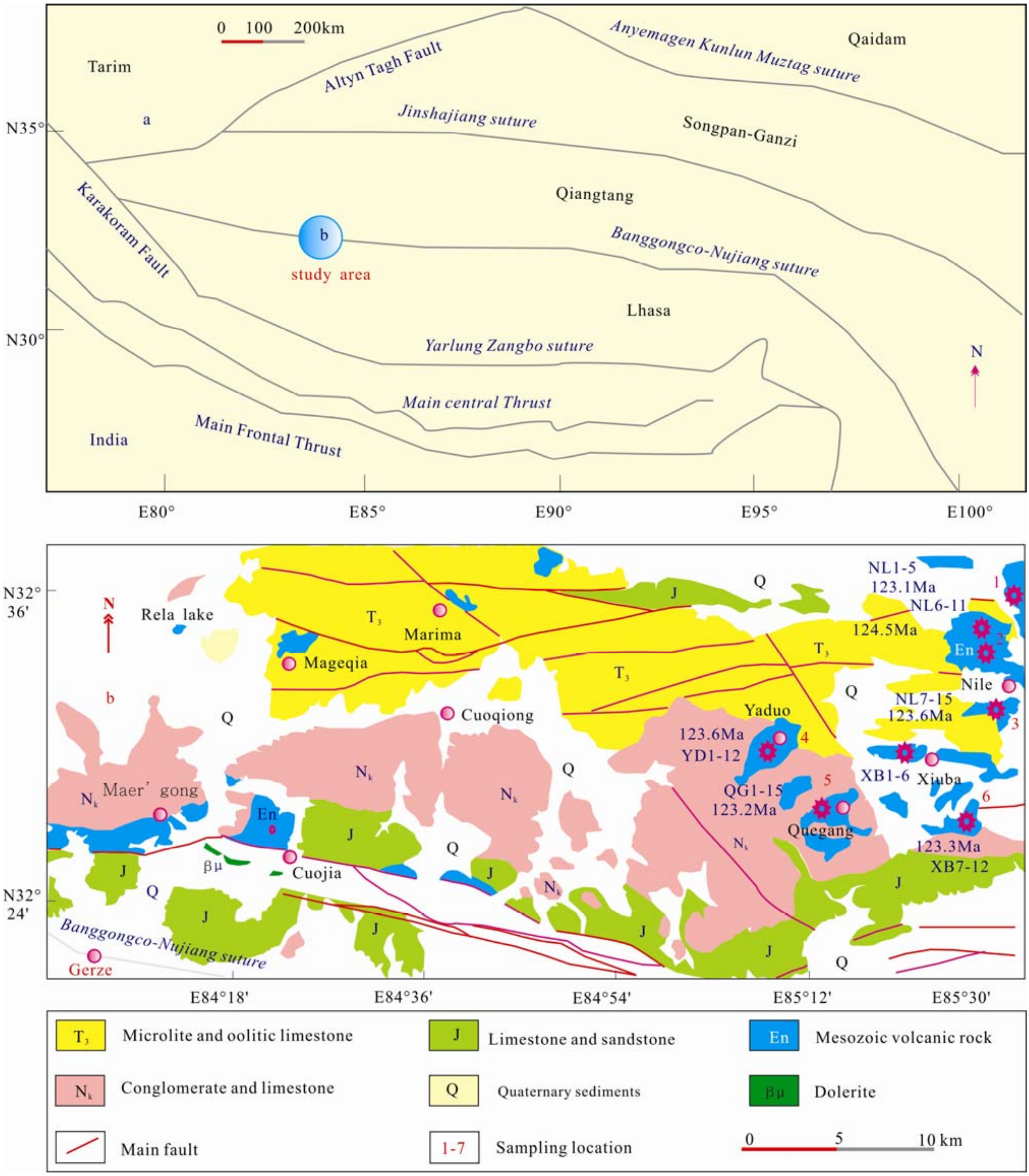

Fig. 1. Geological map of the study area showing the distribution of the volcanic rocks of Mesozoic age across the Gerze region, southern Qiangtang Terrane. Polygonal rings indicate the six sampling sites.

located at Ngari Prefecture, along the southern margin of the Qiangtang Terrane, and adjacent to the Banggongco–Nujiang Suture and Lhasa Terrane (Fig. 1a–b). There are unique lithospheric structures and igneous rock (e.g., mafic to intermediate volcanic rocks) recorded throughout this area. The volcanic rocks are widely distributed, and mainly include: andesite, minor basaltic andesite, and quartz andesite. In contrast, plutonic-intrusive rocks are rarely found. The distribution of volcanic rocks is closely related to tectonic environment (Fig. 1a–b), with those examined as part of this study occurring as expansive lava flows within a continental basin, and that cover an area of 45–60 m^2. The volcanic rocks occur in a sequence that includes microlite and oolitic limestone (T_3), conglomerate and limestone (N_k), and Quaternary (Q) sediments. The volcanic units strike approximately E–W, N–S, and NE (Fig. 1a–b).

3 Samples and Methods

3.1 Samples

Nile County in Gerze is predominantly dark grey, porphyritic and with a massive–type structure (Fig. 2a, e). The phenocryst consists of hypidiomorphic plagioclase (15%–20%), quartz (2.0%–4.0%), and hornblende (0.8%–1.0%). The matrix comprises plagioclase (55%–60%), quartz (5.0%–8.0%), and chlorite (10%–16%). Amphibole is commonly altered to chlorite, while feldspar is sericitised; calcite is also present in the matrix. The volcanic rocks (andesite) from Yaduo county, Gerze are dark grey and greenish grey (Fig. 2b, f), porphyritic and massive in structure. The phenocrysts consist of hypidiomorphic plagioclase (16%–22%), quartz (2.0%–5.0%), and hornblende (0.7%–1.2%). The matrix

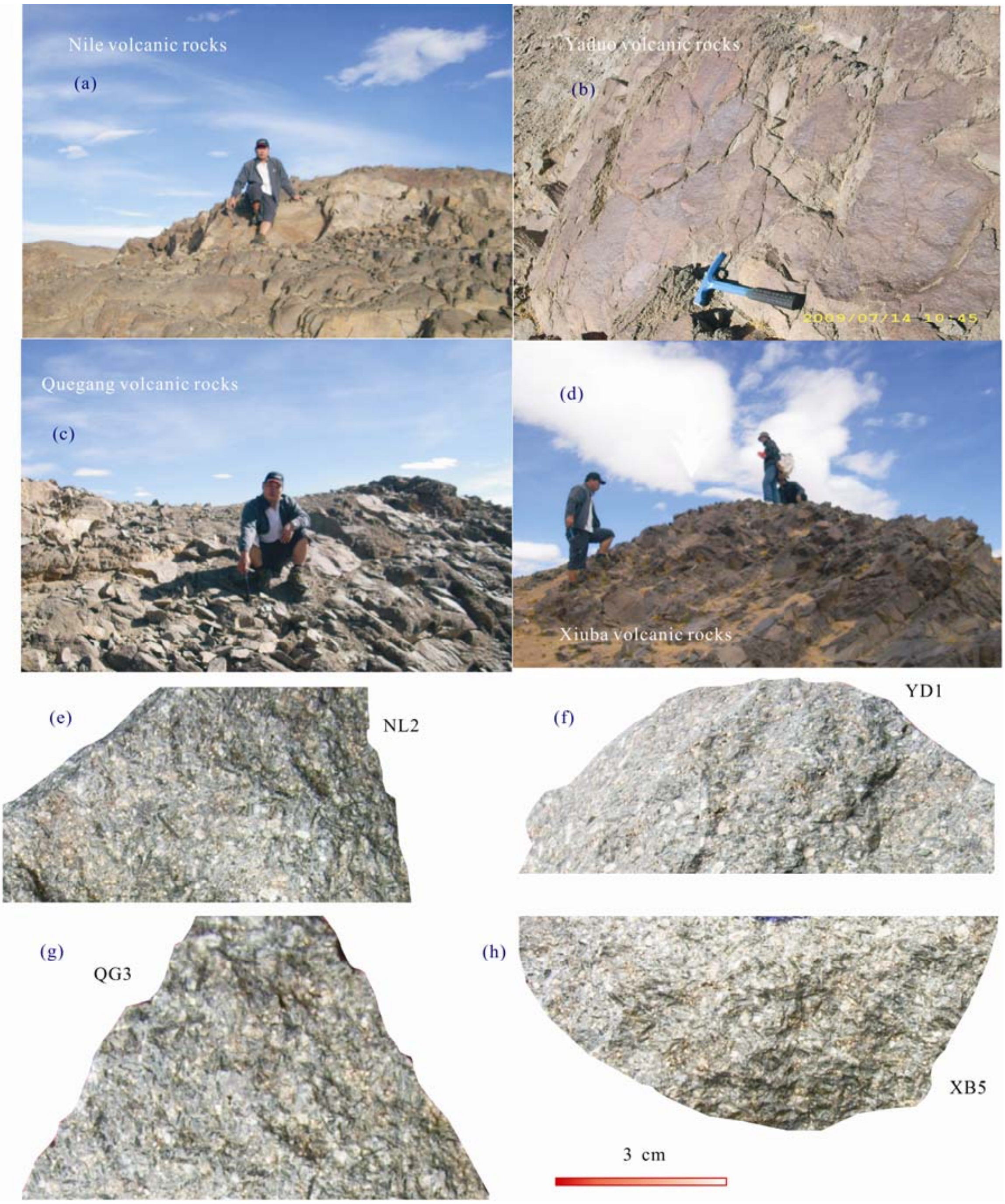

Fig. 2. Representative field and hand specimen photographs showing the main outcrops of the Gerze volcanic rocks from the study area in the southern Qiangtang Terrane, northern Tibet.

comprises plagioclase (55%–60%), quartz (5.0%–7.0%), and chlorite (10%–15%). The volcanic rocks (andesite) from Quegang county, Gerze are dark grey and greenish grey (Fig. 2c, g), porphyritic and massive in structure. Phenocrysts consist of hypidiomorphic plagioclase (15%–21%), quartz (3.0%–5.0%), and hornblende (0.8%–1.1%). The matrix comprises plagioclase (55%–60%), quartz (5.0%–8.0%), chlorite (10%–16%), and minor sericite and calcite. The volcanic rocks (andesite) from Xiuba county, Gerze are dark grey and light green (Fig. 2d, h), porphyritic and massive in structure. The phenocryst consists of hypidiomorphic plagioclase (16%–20%), quartz (2.0%–5.0%), and hornblende (0.9%–1.2%). The matrix comprises plagioclase (56%–60%), quartz (5.0%–9.0%), and chlorite (10%–15%), along with minor sericite and calcite.

3.2 U–Pb dating by LA–ICP–MS

Zircon was separated from six of the collected volcanic samples (NL01, NL03, NL02, YD02, QG04 and XB03), using conventional heavy–liquid and magnetic techniques, at the Langfang Regional Geological Survey, Hebei Province, China. Single grains of zircon were examined under transmitted and reflected light microscopy, and by cathodoluminescence (CL) petrography (Fig. 3) at the State Key Laboratory of Continental Dynamics, Northwest University, China, to reveal their external and internal structures.

Prior to zircon U-Pb dating, grain mount surfaces were washed in dilute HNO_3 and pure alcohol to remove any potential lead contamination. Zircon U-Pb and $^{207}Pb/^{206}Pb$ weighted average ages were determined by LA-ICP-MS (Table 1; Fig. 4); using an Agilent 7500a ICP-MS instrument equipped with a 193 nm excimer laser, at the State Key Laboratory of Continental Dynamics, Northwest University. The zircon standard, 91500 was used for quality control, and a NIST 610 standard was used for data optimization. A spot diameter of 24 mm was used during the analysis, employing the methodologies described by Liu et al. (2010). Common Pb correction was undertaken following the approach of Andersen (2002), and the resulting data were processed using GLITTER and ISOPLOT (Ludwig, 2003; Table 1; Fig. 4). Uncertainties on individual LA-ICP-MS analyses are quoted at the 95% (1s) confidence level.

3.3 Whole–rock major and trace elements

Major oxides were analyzed with a PANalytical Axios-advance X-ray fluorescence spectrometer (XRF) at the State Key Laboratory of Ore Deposit Geochemistry (LODG), Institute of Geochemistry, Chinese Academy of Science (IGCAS). The experimental process is as follows. (1) Calculation of ignition on loss (LOI): Crucible weight is called, 1g samples were added into the crucible, and then the crucible placed in the muffle furnace and keep burning for three hours at a temperature of 900°C, the crucible is cooled and stamped, and then placed in a dryer, subsequently, the samples were weighed for 30 minutes, and the ignition on loss of the sample was calculated. (2) Preparation of sample to be measured: The 0.7 sample and the 7 flux ($Li_2B_4O_7$) are loaded into the crucible, the sample and flux was stirred with glass rods and poured into a platinum crucible, a proper amount of LiBr was added into the platinum crucible, hen then platinum crucible was melted under the condition of 1150°C. The sample melt is poured into the platinum mold, after cooling, flat glass pieces can be tested on the machine. The analytical precision as determined on the Chinese National standard GSR–3, and the detection limit was better than 5%, and the detection limits For GSR-13 is also provided (Table 2). Trace elements were analyzed with a POEMS ICP–MS at the National Research Center of Geoanalysis, Chinese Academy of Geosciences. Fifty milligrams of powdered mafic sample were placed in a Polytetrafluoroethylene bomb. To each sample was added 1 ml of HF (38%) and 0.5 ml of HNO_3 (68%). The bombs were then placed on a hot plate, and the solution evaporated to dryness to remove most of the silica. One milliliter of HF and 0.5 ml of HNO_3 were then added. The sealed bombs were then placed in an electric oven and heated to 190°C for 48 h (overnight). After cooling, the bombs were then opened, 1 ml of 1 μg/ml Rh solution was added as an internal standard and placed on a hot plate (at about 150°C), and the solutions evaporated to dryness. One milliliter of HNO_3 was added, evaporated to dryness and followed by a second addition of HNO_3 and evaporation to dryness. The final residue was re-dissolved by adding 8 ml of 40% HNO_3, resealing the bombs and returning them to the electric oven heated at 110°C for a period of 6 h. After cooling, the final solution was made up to a 100 ml by addition of distilled de-ionized water (Qi et al., 2000). The discrepancy between the triplicates is less than 5% for all the elements. Analyses of international standards OU–6 is in agreement with the recommended values, and the detection limit was better than 5%, and the detection limits for OU–16 is also provided (Table 3).

3.4 Sr-Nd isotopes

For Rb-Sr and Sm-Nd isotope analyses, sample powders were spiked with mixed isotope tracers, dissolved in Teflon capsules with HF+HNO_3 acids, and separated by conventional cation–exchange technique (Zhang et al., 2001). Isotopic measurements were performed using a Finnigan Triton Ti thermal ionization mass spectrometer at

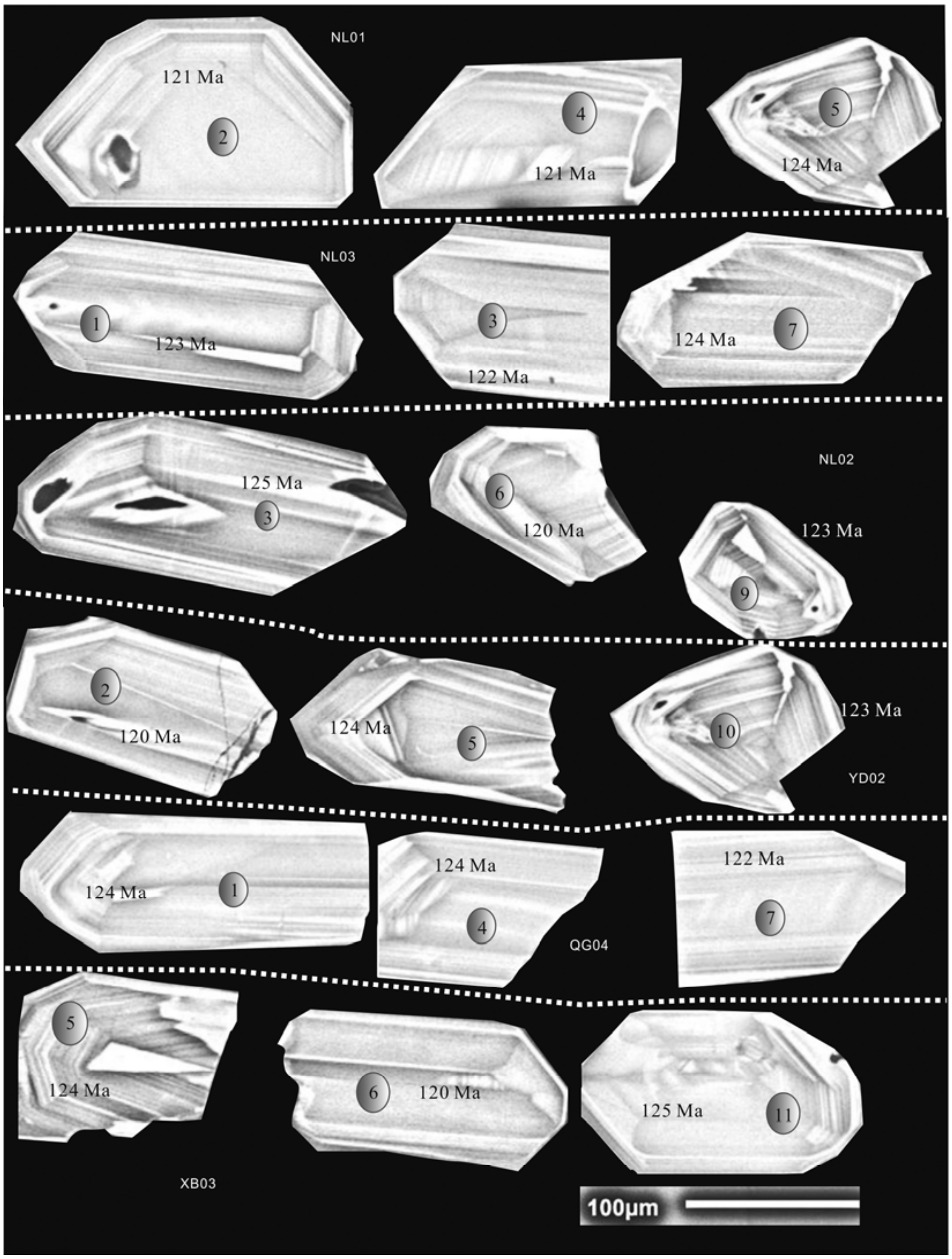

Fig. 3. Representative Cathodoluminescence (CL) images of zircon grains within the Gerze volcanic rock samples (NL01, NL03, NL02, YD02, QG04 and XB03) from the study area in the southern Qiangtang Terrane, northern Tibet.

the State Key Laboratory of Geological Processes and Mineral Resources, China. Procedural blanks yielded concentrations of <200 pg for Sm and Nd and <500 pg for Rb and Sr, and mass fractionation corrections for Sr and Nd isotopic ratios were based on $^{86}Sr/^{88}Sr$=0.1194 and $^{146}Nd/^{144}Nd$=0.7219, respectively. Analysis of the NBS987 and La Jolla standards yielded values of $^{87}Sr/^{86}Sr$=0.710246±16 (2s), and $^{143}Nd/^{144}Nd$ =0.511863±8 (2s), respectively.

4 Results

4.1 LA-ICP-MS U-Pb age dating

Euhedral zircon grains in samples NL01, NL03, NL02, YD02, QG04 and XB03 are clean and prismatic, with magmatic oscillatory zoning (Fig. 3), indicative of a

Table 1 LA-ICP-MS Zircon U-Pb isotopic data of volcanic rocks, southern Qiangtang Terrane, Gerze, northern Tibet

NL01					Isotopic	Ratios					Age (Ma)					
Spot	Th (ppm)	U (ppm)	Pb (ppm)	Th/U	$^{207}Pb/^{206}Pb$	1δ	$^{207}Pb/^{235}U$	1δ	$^{206}Pb/^{238}U$	1δ	$^{207}Pb/^{206}Pb$	1δ	$^{207}Pb/^{235}U$	1δ	$^{206}Pb/^{238}U$	1δ
1	75	113	43.5	0.66	0.11007	0.00152	5.25166	0.07419	0.34514	0.00217	1801	17	1861	12	1911	10
2	134	166	4.23	0.81	0.0481	0.00356	0.12612	0.00916	0.01902	0.00026	104	136	121	8	121	2
3	276	255	6.22	1.08	0.04605	0.00355	0.12054	0.00916	0.01898	0.00025		141	116	8	121	2
4	223	198	4.82	1.13	0.05044	0.00427	0.13229	0.01106	0.01902	0.00026	215	164	126	10	121	2
5	656	1013	27.4	0.65	0.04741	0.00129	0.12708	0.00358	0.01941	0.0002	70	47	121	3	124	1
6	278	531	18.1	0.52	0.04609	0.00147	0.12316	0.00367	0.01945	0.00015	2	46	118	3	124	0.9
7	198	194	4.73	1.02	0.05088	0.00627	0.13226	0.01617	0.01885	0.00028	235	246	126	15	120	2
8	293	504	21.2	0.58	0.04924	0.00144	0.1315	0.00357	0.01937	0.00021	159	43	125	3	124	1
9	376	605	17.4	0.62	0.04773	0.00158	0.12686	0.00393	0.01933	0.00024	86	49	121	4	123	2
10	269	531	18.2	0.51	0.05079	0.0015	0.13575	0.00389	0.01941	0.00021	231	46	129	3	124	1
11	425	372	9.55	1.14	0.04832	0.00262	0.12901	0.00709	0.01935	0.00023	115	101	123	6	124	1
12	246	291	6.57	0.85	0.05547	0.004	0.14512	0.0111	0.01916	0.00042	431	132	138	10	122	3
13	426	338	8.53	1.26	0.04651	0.00396	0.11533	0.00971	0.01884	0.00032	24	153	111	9	120	2
14	137	288	15.4	0.48	0.04725	0.00465	0.12311	0.01207	0.0189	0.00018	62	198	118	11	121	1
NL03					Isotopic	Ratios					Age (Ma)					
Spot	Th (ppm)	U (ppm)	Pb (ppm)	Th/U	$^{207}Pb/^{206}Pb$	1δ	$^{207}Pb/^{235}U$	1δ	$^{206}Pb/^{238}U$	1δ	$^{207}Pb/^{206}Pb$	1 δ	$^{207}Pb/^{235}U$	1δ	$^{206}Pb/^{238}U$	1δ
1	322	289	6.88	1.11	0.04914	0.00224	0.12742	0.00596	0.01927	0.00039	155	71	122	5	123	2
2	286	483	11.3	0.59	0.04606	0.0021	0.12258	0.00542	0.0194	0.0002	1	74	117	5	124	1
3	365	362	7.96	1.01	0.05713	0.0047	0.1461	0.01353	0.01913	0.00051	497	158	138	12	122	3
4	386	343	8.55	1.13	0.05221	0.0027	0.13814	0.00709	0.01919	0.0002	295	99	131	6	123	1
5	241	233	5.71	1.03	0.0486	0.00227	0.12781	0.00569	0.01928	0.00024	129	79	122	5	123	2
6	414	353	8.69	1.17	0.0484	0.00181	0.12924	0.0048	0.01935	0.00018	119	69	123	4	124	1
7	157	246	104	0.64	0.11172	0.00138	5.17904	0.06693	0.33535	0.002	1828	15	1849	11	1864	10
8	243	405	9.14	0.60	0.04976	0.00212	0.13274	0.00549	0.01947	0.0002	184	77	127	5	124	1
9	342	651	23.2	0.53	0.04905	0.00114	0.13353	0.00312	0.01971	0.00014	150	41	127	3	126	0.9
10	145	194	4.64	0.75	0.04962	0.0047	0.13301	0.01247	0.01944	0.00026	177	186	127	11	124	2
11	218	335	7.62	0.65	0.05217	0.00173	0.14241	0.0047	0.01985	0.00022	293	55	135	4	127	1
12	135	208	85.3	0.65	0.11397	0.00142	5.33481	0.0725	0.33901	0.00263	1864	14	1874	12	1882	12
13	275	348	8.24	0.79	0.05651	0.00242	0.15272	0.00638	0.01941	0.00025	472	70	144	6	124	2
14	84.3	119	3.36	0.71	0.13702	0.01073	0.3495	0.02715	0.01943	0.00052	2190	98	304	20	124	3
NL02					Isotopic	Ratios					Age (Ma)					
Spot	Th (ppm)	U (ppm)	Pb (ppm)	Th/U	$^{207}Pb/^{206}Pb$	1δ	$^{207}Pb/^{235}U$	1δ	$^{206}Pb/^{238}U$	1δ	$^{207}Pb/^{206}Pb$	1δ	$^{207}Pb/^{235}U$	1δ	$^{206}Pb/^{238}U$	1δ
1	1535	986	54.5	1.5568	0.0525	0.0028	0.1225	0.0058	0.0195	0.0003	307	80	117	5	124	2
2	637	421	25.2	1.51306	0.0516	0.0027	0.1233	0.0058	0.0188	0.0004	268	69	118	5	120	3
3	873	617	43.3	1.41491	0.0518	0.0025	0.1254	0.0058	0.0196	0.0003	277	78	120	5	125	2
4	553	628	28.2	0.88057	0.0462	0.0027	0.1253	0.0072	0.0194	0.0003	8	94	120	6	124	2
5	512	387	56.4	1.323	0.0518	0.0029	0.1236	0.0055	0.0195	0.0003	277	74	118	5	124	2
6	95.3	73.6	6.65	1.29484	0.0526	0.0027	0.1247	0.0056	0.0188	0.0003	312	73	119	5	120	2
7	408	415	358	0.98313	0.0525	0.0028	0.1234	0.0055	0.0192	0.0003	307	73	118	5	123	2
8	1316	952	75.5	1.38235	0.0526	0.0028	0.1235	0.0056	0.0198	0.0003	312	75	118	5	126	2
9	526	267	19.5	1.97004	0.0524	0.0027	0.1228	0.0061	0.0192	0.0003	303	85	118	6	123	2
10	1031	375	76.6	2.74933	0.0522	0.0024	0.1232	0.0062	0.0192	0.0003	294	86	118	6	123	2
11	1038	562	132	1.84698	0.0522	0.0025	0.1226	0.0061	0.0195	0.0003	294	85	117	6	124	2
12	629	297	48.8	2.11785	0.0524	0.0024	0.1222	0.0055	0.0196	0.0003	303	75	117	5	125	2

Continued Table 1

YD02					Isotopic Ratios						Age (Ma)					
Spot	Th (ppm)	U (ppm)	Pb (ppm)	Th/U	$^{207}Pb/^{206}Pb$	1δ	$^{207}Pb/^{235}U$	1δ	$^{206}Pb/^{238}U$	1δ	$^{207}Pb/^{206}Pb$	1δ	$^{207}Pb/^{235}U$	1δ	$^{206}Pb/^{238}U$	1δ
1	928	964	75.1	0.96	0.0526	0.0027	0.1226	0.0058	0.0196	0.0003	312	80	117	5	125	2
2	572	484	43.7	1.18	0.0517	0.0028	0.1234	0.0056	0.0188	0.0004	272	65	118	5	120	3
3	896	714	46.5	1.25	0.0518	0.0025	0.1253	0.0058	0.0195	0.0003	277	78	120	5	124	2
4	521	633	33.5	0.82	0.0463	0.0028	0.1253	0.0072	0.0195	0.0004	13	85	120	6	124	3
5	482	356	72.6	1.35	0.0518	0.0029	0.1235	0.0056	0.0194	0.0003	277	75	118	5	124	2
6	114	69.7	9.38	1.64	0.0525	0.0028	0.1246	0.0056	0.0188	0.0003	307	73	119	5	120	2
7	384	432	217	0.89	0.0526	0.0027	0.1235	0.0055	0.0191	0.0004	312	64	118	5	122	3
8	969	986	78.2	0.98	0.0525	0.0027	0.1235	0.0055	0.0198	0.0003	307	74	118	5	126	2
9	407	325	24.1	1.25	0.0525	0.0027	0.1228	0.0062	0.0192	0.0003	307	86	118	6	123	2
10	824	565	95.4	1.46	0.0522	0.0025	0.1233	0.0062	0.0192	0.0004	294	77	118	6	123	3
11	822	579	156	1.42	0.0521	0.0024	0.1225	0.0061	0.0196	0.0003	290	86	117	6	125	2
12	517	343	66.5	1.51	0.0525	0.0025	0.1221	0.0056	0.0195	0.0003	307	76	117	5	124	2

QG04					Isotopic Ratios						Age (Ma)					
Spot	Th (ppm)	U (ppm)	Pb (ppm)	Th/U	$^{207}Pb/^{206}Pb$	1δ	$^{207}Pb/^{235}U$	1δ	$^{206}Pb/^{238}U$	1δ	$^{207}Pb/^{206}Pb$	1 δ	$^{207}Pb/^{235}U$	1 δ	$^{206}Pb/^{238}U$	1 δ
1	436	465	412	0.94	0.0555	0.0028	0.1226	0.0056	0.0195	0.0003	432	74	117	5	124	2
2	185	145	112	1.28	0.0516	0.0027	0.1233	0.0056	0.0186	0.0004	268	65	118	5	119	3
3	68.2	73.5	16.5	0.93	0.0517	0.0025	0.1253	0.0058	0.0196	0.0003	272	78	120	5	125	2
4	305	246	29.4	1.24	0.0463	0.0027	0.1254	0.0073	0.0195	0.0004	13	87	120	7	124	3
5	384	372	31.3	1.03	0.0518	0.0028	0.1236	0.0056	0.0194	0.0003	277	75	118	5	124	2
6	512	424	72.6	1.21	0.0525	0.0028	0.1248	0.0056	0.0188	0.0003	307	73	119	5	120	2
7	133	124	13.5	1.07	0.0525	0.0027	0.1236	0.0055	0.0191	0.0003	307	73	118	5	122	2
8	242	189	25.5	1.28	0.0526	0.0028	0.1235	0.0054	0.0197	0.0003	312	72	118	5	126	2
9	414	266	174	1.56	0.0525	0.0026	0.1288	0.0062	0.0192	0.0003	307	81	123	6	123	2
10	153	149	10.4	1.03	0.0522	0.0024	0.1234	0.0061	0.0193	0.0003	294	84	118	6	123	2
11	197	136	17.5	1.45	0.0521	0.0024	0.1225	0.0062	0.0195	0.0003	290	87	117	6	124	2

XB03					Isotopic Ratios						Age (Ma)					
Spot	Th (ppm)	U (ppm)	Pb (ppm)	Th/U	$^{207}Pb/^{206}Pb$	1δ	$^{207}Pb/^{235}U$	1δ	$^{206}Pb/^{238}U$	1δ	$^{207}Pb/^{206}Pb$	1 δ	$^{207}Pb/^{235}U$	1 δ	$^{206}Pb/^{238}U$	1 δ
1	321	455	392	0.71	0.0556	0.0027	0.1225	0.0055	0.0196	0.0004	436	64	117	5	125	3
2	166	172	124	0.97	0.0515	0.0028	0.1234	0.0056	0.0186	0.0004	263	65	118	5	119	3
3	72.2	78.4	20.5	0.92	0.0516	0.0026	0.1252	0.0056	0.0195	0.0003	268	74	120	5	124	2
4	283	264	33.7	1.07	0.0462	0.0028	0.1254	0.0072	0.0195	0.0004	8	85	120	6	124	3
5	358	393	34.4	0.91	0.0518	0.0028	0.1235	0.0055	0.0195	0.0003	277	74	118	5	124	2
6	486	435	75.2	1.12	0.0526	0.0027	0.1248	0.0055	0.0188	0.0004	312	62	119	5	120	3
7	149	108	16.7	1.38	0.0525	0.0028	0.1235	0.0056	0.0192	0.0003	307	75	118	5	123	2
8	219	166	28.1	1.32	0.0525	0.0027	0.1236	0.0055	0.0196	0.0003	307	73	118	5	125	2
9	427	239	191	1.79	0.0526	0.0025	0.1286	0.0061	0.0192	0.0004	312	70	123	5	123	3
10	174	123	14.6	1.41	0.0522	0.0024	0.1235	0.0062	0.0192	0.0003	294	86	118	6	123	2
11	228	142	21.2	1.61	0.0522	0.0025	0.1226	0.0062	0.0196	0.0003	294	87	117	6	125	2

Table 2 Whole-rock major element compositions (wt%) of representative volcanic rocks, southern Qiangtang Terrane, Gerze, northern Tibet

Sample	SiO_2	TiO_2	Al_2O_3	Fe_2O_3	MnO	MgO	CaO	Na_2O	K_2O	P_2O_5	LOI	Total	$Mg^{\#}$
NL1	57.34	0.62	16.26	6.45	0.12	2.45	5.16	3.82	2.96	0.26	3.73	99.17	43
NL2	57.52	0.62	16.33	6.41	0.15	2.55	4.48	5.18	2.53	0.25	3.28	99.30	44
NL3	57.48	0.61	16.51	6.76	0.16	2.75	5.81	4.24	2.31	0.28	2.62	99.53	45
NL4	57.65	0.63	16.45	6.74	0.15	2.53	5.65	4.18	2.23	0.26	2.86	99.33	43
NL5	58.65	0.85	15.92	6.42	0.16	2.25	3.85	4.36	3.05	0.33	3.42	99.26	41
NL6	58.58	0.83	15.85	6.36	0.15	2.72	3.89	3.91	2.74	0.31	3.84	99.18	46
NL7	58.56	0.84	16.05	7.14	0.16	2.69	4.34	3.67	2.94	0.28	2.55	99.22	43
NL8	58.47	0.83	15.85	6.86	0.15	2.48	4.93	4.23	3.15	0.28	2.12	99.35	42
NL9	58.82	0.83	15.82	6.21	0.16	2.91	3.03	4.65	3.12	0.31	3.29	99.15	48
NL10	58.86	0.82	15.67	6.25	0.18	3.35	2.86	4.28	3.06	0.28	3.51	99.12	51
NL11	58.64	0.83	15.89	6.43	0.16	3.43	3.72	4.31	3.13	0.32	2.37	99.23	51
NL12	58.33	0.83	15.81	6.41	0.18	3.38	2.92	4.39	3.18	0.33	3.35	99.11	51
NL13	57.76	0.82	15.83	6.23	0.16	3.18	3.73	5.27	3.24	0.31	2.68	99.21	50
NL14	58.54	0.83	15.86	6.25	0.16	3.04	3.92	5.03	3.08	0.28	2.44	99.43	49
NL15	58.18	0.84	16.24	6.43	0.16	2.55	4.52	4.13	3.18	0.28	2.73	99.24	44
YD1	57.65	0.83	15.76	6.36	0.16	2.57	4.34	4.16	3.28	0.32	3.71	99.14	44
YD2	58.62	0.84	16.24	6.46	0.15	2.43	4.28	4.23	2.91	0.31	2.92	99.39	43
YD3	57.78	0.84	16.17	6.54	0.15	2.41	5.06	3.85	2.84	0.28	3.29	99.21	42
YD4	58.54	0.83	16.08	6.44	0.16	2.35	4.34	4.32	2.83	0.28	3.18	99.35	42
YD5	58.25	0.84	16.04	6.42	0.16	2.44	4.48	4.18	2.82	0.29	3.31	99.23	43
YD6	58.43	0.83	16.09	6.64	0.16	2.38	5.09	3.84	2.72	0.28	2.93	99.39	42
YD7	58.23	0.84	16.18	6.52	0.15	2.14	5.45	3.95	2.59	0.32	2.87	99.24	39
YD8	58.54	0.84	16.11	6.54	0.16	2.36	5.23	3.46	2.71	0.32	3.05	99.32	42
YD9	58.31	0.82	15.76	6.09	0.16	2.28	6.28	3.65	2.73	0.29	3.04	99.41	29
YD10	58.72	0.83	16.18	6.36	0.16	2.15	5.74	4.18	2.63	0.28	2.25	99.48	40
YD11	58.18	0.83	16.05	6.09	0.16	2.34	4.68	5.07	2.43	0.28	3.26	99.37	43
YD12	58.91	0.84	16.08	6.55	0.18	2.41	4.93	3.64	2.65	0.28	2.78	99.25	42
QG1	58.32	0.84	16.33	6.65	0.16	2.46	4.05	4.14	2.92	0.33	3.24	99.44	42
QG2	58.26	0.83	15.73	6.16	0.15	1.92	5.45	4.28	3.12	0.31	3.15	99.36	38
QG3	58.28	0.84	15.85	6.29	0.15	2.39	4.64	4.65	3.07	0.28	3.05	99.49	43
QG4	58.19	0.83	15.86	6.35	0.16	2.34	4.65	3.94	3.09	0.31	3.45	99.17	42
QG5	58.76	0.82	15.88	5.92	0.15	2.36	4.93	4.38	3.08	0.29	2.81	99.38	44
QG6	58.38	0.80	15.82	5.90	0.14	2.79	3.40	4.80	2.85	0.28	4.26	99.41	48
QG7	58.68	0.82	15.85	5.86	0.15	2.38	4.73	4.36	3.07	0.28	3.21	99.39	45
QG8	58.79	0.82	15.86	5.93	0.15	2.38	4.86	4.43	3.05	0.28	2.63	99.18	44
QG9	58.75	0.83	15.87	5.96	0.16	2.36	4.95	4.38	3.08	0.29	2.72	99.35	44
QG10	58.84	0.82	16.04	6.12	0.15	2.28	4.65	4.06	2.96	0.29	3.25	99.46	42
QG11	59.31	0.85	15.68	5.82	0.14	2.32	4.55	4.16	2.86	0.26	3.23	99.18	44
QG12	58.76	0.83	15.76	6.14	0.13	2.48	4.49	4.27	2.88	0.29	3.36	99.39	44
QG13	58.62	0.79	16.06	6.16	0.15	2.45	4.36	4.33	3.25	0.29	2.75	99.21	44
QG14	59.74	0.81	15.57	5.73	0.14	2.04	3.94	5.15	2.95	0.29	3.03	99.39	41
QG15	58.46	0.65	16.03	6.34	0.15	2.52	5.53	5.22	2.08	0.28	1.96	99.22	44
XB1	58.57	0.73	16.35	6.55	0.14	2.59	5.75	4.73	1.44	0.26	2.35	99.46	44
XB2	58.36	0.64	16.34	6.43	0.15	2.72	5.38	4.54	2.16	0.25	2.45	99.42	46
XB3	58.67	0.76	16.16	6.54	0.16	2.84	5.57	4.23	2.12	0.26	2.15	99.46	46
XB4	59.75	0.86	16.19	6.08	0.15	2.28	1.56	6.06	2.94	0.28	3.12	99.27	43
XB5	58.65	0.84	15.87	6.09	0.15	2.46	3.76	4.94	3.15	0.28	3.16	99.35	44
XB6	58.86	0.83	16.26	6.32	0.15	2.55	4.24	6.05	1.74	0.26	1.94	99.20	44
XB7	58.56	0.65	16.41	6.54	0.15	2.65	5.16	4.93	2.05	0.26	2.13	99.49	45
XB8	58.46	0.62	16.52	6.53	0.15	2.54	4.26	5.22	2.05	0.25	2.76	99.36	44
XB9	58.68	0.63	16.43	6.72	0.15	2.43	5.63	3.82	2.11	0.25	2.54	99.39	42
XB10	58.72	0.63	16.45	6.42	0.15	2.45	4.39	5.41	2.03	0.26	2.26	99.17	43
XB11	58.55	0.62	16.36	6.37	0.14	2.58	4.42	5.74	2.04	0.25	2.44	99.51	45
XB12	58.28	1.05	15.06	6.63	0.16	2.62	5.93	4.65	2.34	0.26	2.15	99.13	44

LOI: loss on ignition. $Mg^{\#}$=100×Mg/(Mg+ΣFe) atomic ratio. RV*: recommended values; MV*: measured values; values for GSR-1 and GSR-3 are from Wang et al. (2003).

magmatic origin. None of the grains show evidence of inherited cores and all have relatively high Th/U ratios (0.48–2.75 for the Nile volcanic rocks, 0.82–1.51 for the Yaduo volcanic rocks, 0.93–1.45 for the Quegang volcanic rocks, and 0.71–1.79 for the Xiuba volcanic rocks), which also favors a magmatic origin. The zircon U-Pb age data indicate that the Nile volcanic rocks were emplaced at between 124.5±0.89 Ma (n=12, MSWD=1.2) and 123.1±0.94 Ma (n=13, MSWD=1.4), the Yaduo volcanic rocks at 123.6±1.3 Ma (n=12, MSWD=0.70), the Quegang volcanic rocks at 123.3±1.2 Ma (n=12, MSWD=0.82), and the Xiuba volcanic rocks at 123.3±1.2 Ma (n=12, MSWD=0.82) (Fig. 4a–f). As such, these Mesozoic igneous rocks were erupted more or less coevally, during the eearly Cretaceous.

4.2 Major and trace elements

The whole-rock major and trace data for the Gerze area volcanic rocks sampled during this study are listed in Supplementary Tables 2 and 3, respectively. These

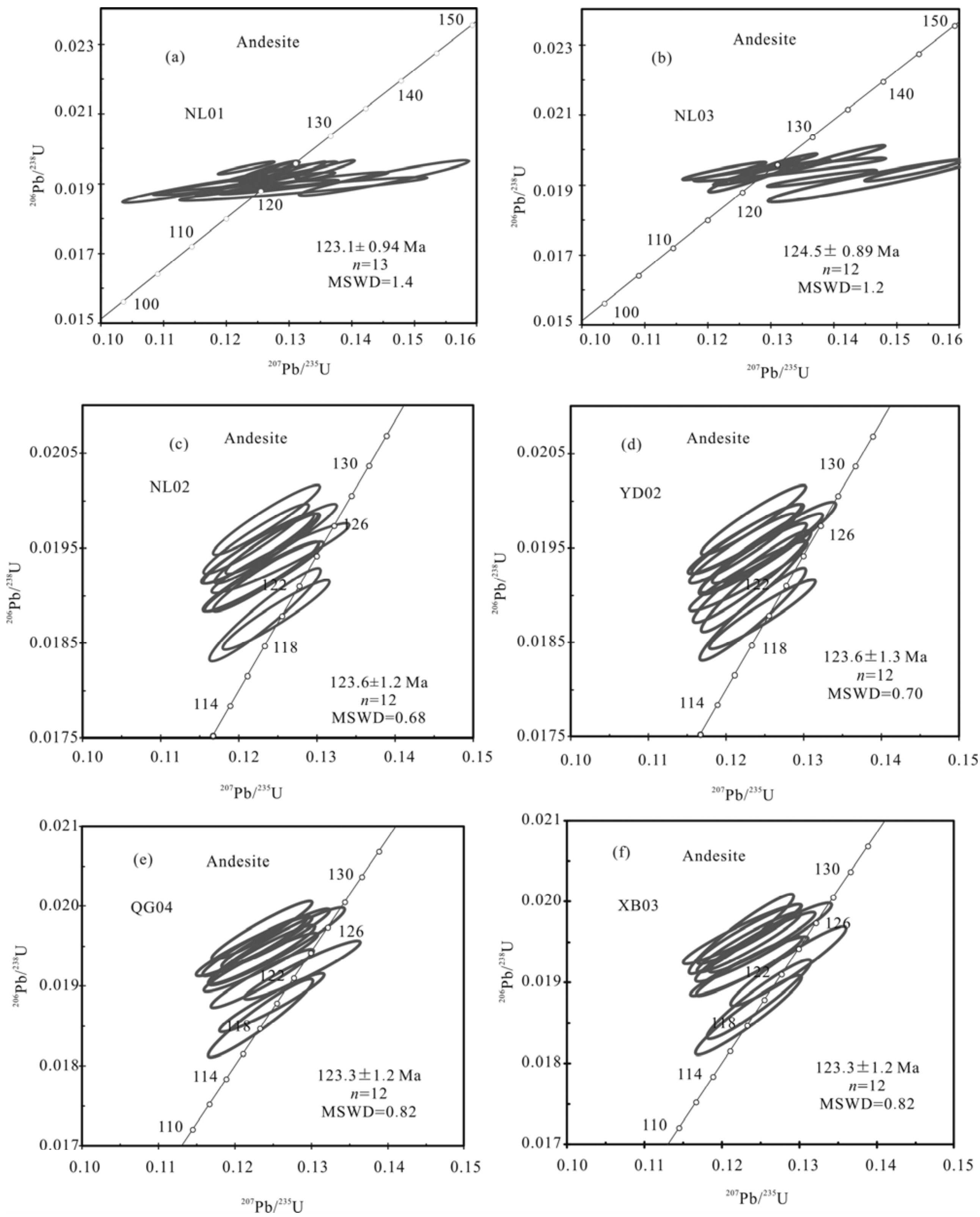

Fig. 4. LA-ICP-MS zircon U-Pb concordia diagrams for volcanic rocks, Gerze, southern Qiangtang Terrane, northern Tibet.

intermediate igneous rocks have relatively uniform compositions, with SiO_2=57.34%–59.74%, TiO_2=0.61%–0.85% (except sample XB12, TiO_2=1.05), Al_2O_3=15.06%–16.52%, Fe_2O_3=5.86%–6.72%, MnO=0.12%–0.18%, MgO=1.92%–3.38%, CaO=1.56%–6.28%, Na_2O=3.46%–6.06%, K_2O=1.44%–3.18%, and P_2O_5=0.25%–0.3%. Most of the volcanic rocks are classified as alkaline (shoshonitic) on a total alkali-silica diagram (Fig. 5a) and as shoshonitic in the Na_2O vs. K_2O diagram (Fig. 5b). These volcanic rocks have poor correlations between SiO_2 and Al_2O_3, TiO_2, Na_2O+K_2O, P_2O_5, MnO, Cr, Ni, and Ba (Fig. 6a, b, d, g, h, 7a, b, f). By contrast, good correlations are observed between SiO_2 and Fe_2O_3, MgO, CaO, Pb, Ta, Rb, Sr, and Zr (Fig. 6c, e, f, 7c, d, e, g, h). The rocks exhibit strong light rare earth element-enrichment (LREE), with a significant range in $(La/Yb)_N$ (34.9–49.5), Sr (671–1432 ppm) and Ba (442–1642 ppm), and a small range in Eu/Eu* (0.19–0.24) values (Table 3; Fig. 8a, b). In addition, the volcanic rocks are characterized by variable $Mg^{\#}$ (29–51), enrichment in large ion lithophile elements (e.g., Rb, Ba, Th, U, K, Pb and Sr), and depletion in high field strength elements (HFSE; Nb, Ta, Hf, and Ti) in primitive mantle–normalized multi–element variation diagrams (Fig. 8a, b).

4.3 Sr-Nd isotopes

The Sr-Nd isotopic compositions of twenty six representative volcanic rocks from the Gerze study area were determined during this investigation (Table 4). These volcanic rocks have a relatively wide range of $(^{87}Sr/^{86}Sr)_i$ values (0.7049–0.7057) and have negative $e_{Nd}(t)$ values (−0.89 to −2.89; Table 4; Fig. 9), indicative of a magma source that is found within an enriched mantle. The Sr-Nd isotopes of the studied samples overlap with those of the Qiangtang potassium volcanic rocks (Liu et al., 2008).

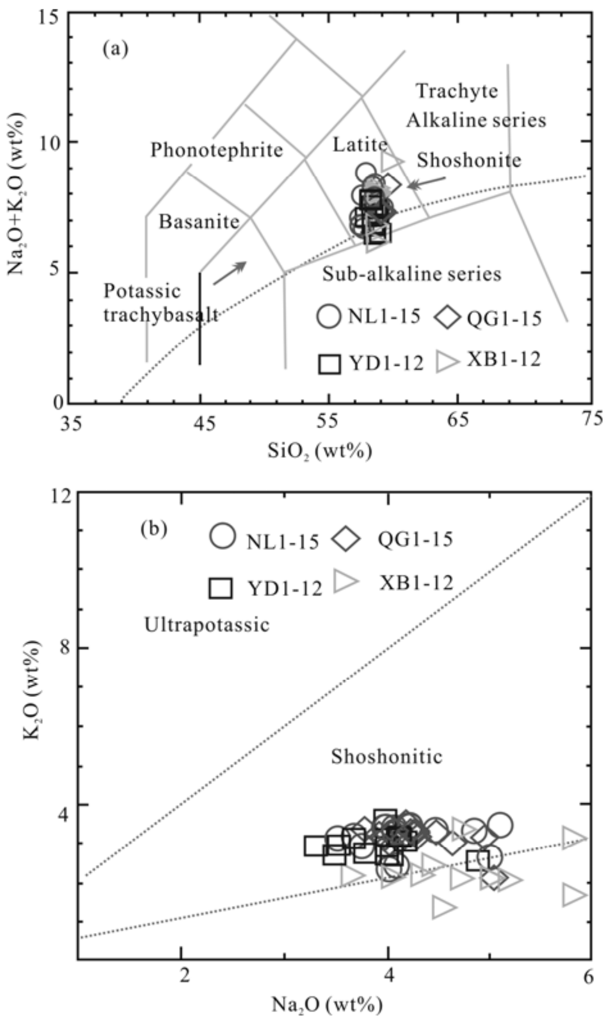

Fig. 5. Plots of whole rock (a) SiO_2 vs. Na_2O+K_2O and (b) Na_2O vs. K_2O for volcanic rocks from the Gerze study area, southern Qiangtang Terrane, northern Tibet.

5 Discussions

5.1 Emplacement age and fractional crystallization

Based on the evidence presented in work from the Tibet Geological Survey Institute (2005), the volcanic rocks of the Gerze region are the products of magmatic activity in the Paleogene; however, geochronological investigations on the volcanic rocks from five regions adjacent to Gerze, have shown those volcanic rocks were instead erupted during the eearly Cretaceous. This is further supported in the U-Pb dating results of this study, i.e., the volcanic rocks from eastern Gerze also were formed during the eearly Cretaceous (74–126 Ma). Our new geochronological framework thus redefines the period of magmatism for volcanic rocks occurring across the Gerze region of northern Tibet.

For the volcanic rocks under investigation, these exhibit a wide range of MgO=1.92%–3.38% contents, and their $Mg^{\#}$ values ($Mg^{\#}$=29–51), however, are significantly lower than that of a primary or a more primitive magma ($Mg^{\#}$=66–75), indicating that the magma of the volcanic rock studied has undergone clear fractionation (Pan Rong et al., 2013). SiO_2 shows a negative correlation with Fe_2O_3, MgO, CaO (Fig. 6c, e, f), Pb, and Ta (Fig. 7c, d), that suggests possible fractionation of clinopyroxene, hornblende, Ti–bearing phases (rutile, ilmenite, titanite, etc.), biotite, plagioclase, zircon, and potassium–feldspar. This is further supported in the observed negative Eu anomalies (Eu/Eu^*=0.19–0.24), and the plots between TiO_2 vs. Zr, Sr vs. Ba, Rb, and Ba/Sr ratio (Fig. 10a–d). The negative Ti anomalies in all volcanic rocks (Fig. 8b) also favor the fractionation of Fe-Ti oxides, such as rutile and limonite. The negative correlation between MgO and Al_2O_3 (data not shown) suggests that plagioclase is not a major fractionating phase for the volcanic rocks studied, which is further supported by the lack of negative Sr anomalies (Fig. 8b).

Most of the investigated Gerze volcanic rocks show a decrease of Zr with increasing SiO_2 (Fig. 7h), implying that zircon was saturated in the magma and was also an important fractionating phase (Li et al., 2007). Zircon saturation thermometry (Watson and Harrison, 1983) provides a simple and robust means of estimating the

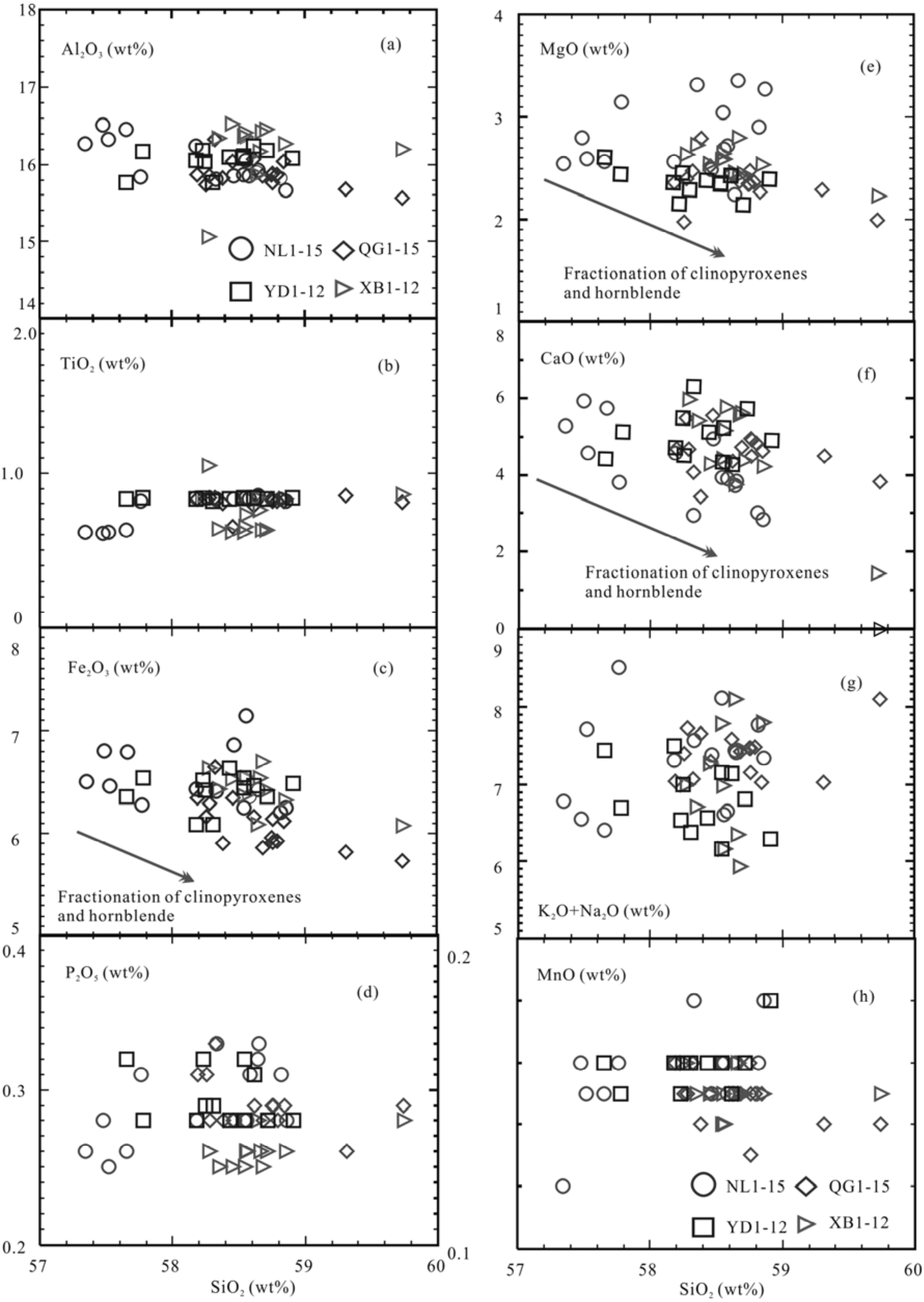

Fig. 6. Plots of whole rock: SiO_2 vs. Al_2O_3, TiO_2, Fe_2O_3, P_2O_5, MgO, CaO, K_2O+Na_2O, and MnO for the volcanic rocks from the Gerze study area, southern Qiangtang Terrane, northern Tibet.

temperature of felsic magma from bulk-rock compositions. The calculated zircon saturation temperatures (tZr°C) of the studied volcanic rocks range from 783 to 874°C (Table 2), which is most likely a minimum temperature of formation.

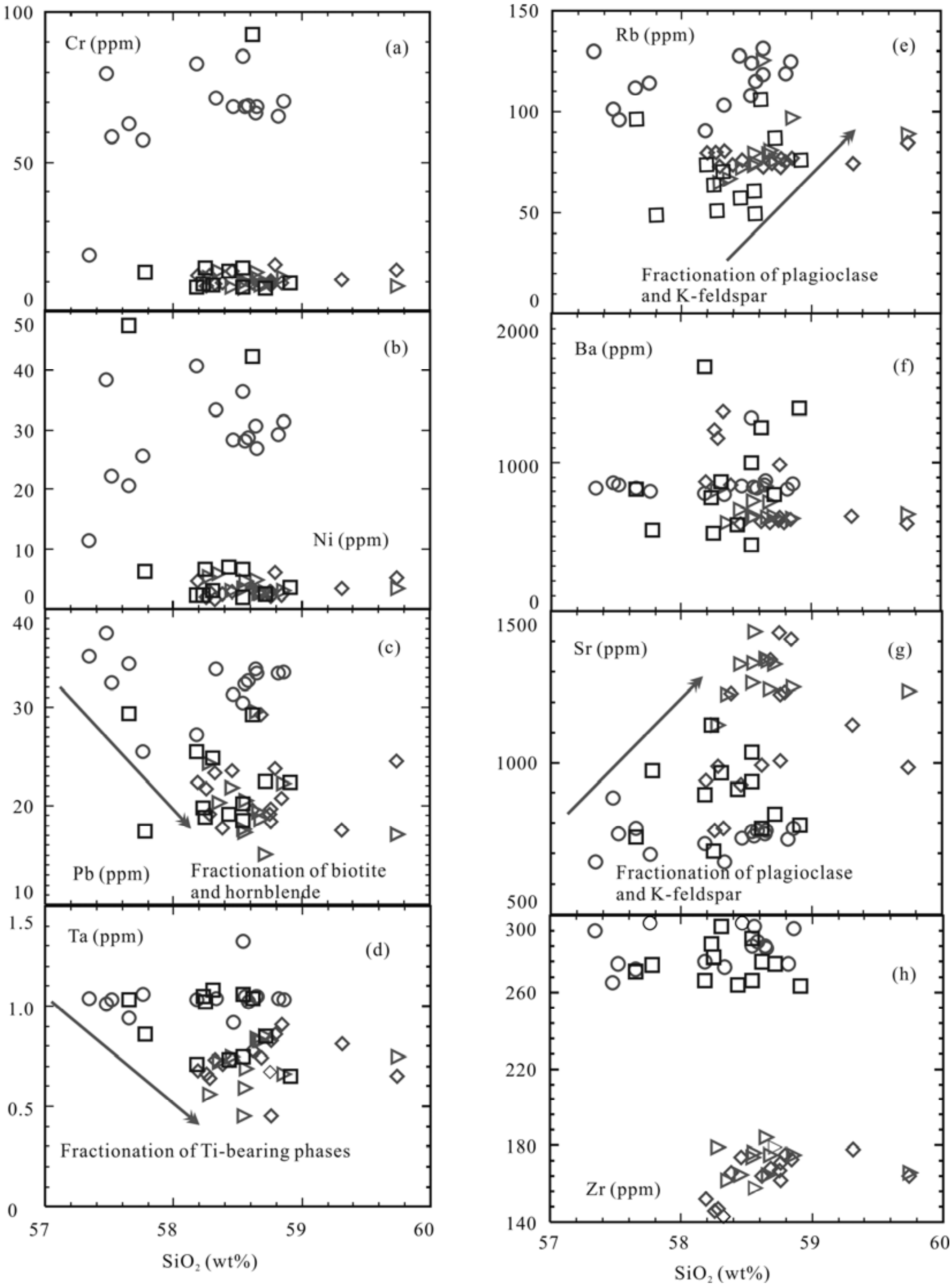

Fig. 7. (a–h), Plots of whole rock : SiO_2 (%) vs. Cr, Ni, Pb, Ta, Rb, Ba, Sr, and Zr for the volcanic rocks from the Gerze study area, southern Qiangtang Terrane, northern Tibet.

5.2 Crustal contamination

It is plausible that the Gerze volcanic rocks investigated herein may have experienced some degree of crustal contamination during ascent and/or residence within crustal magma chambers. It is necessary, therefore, to evaluate the extent of any crustal contamination. Geochemical characteristics, including significant depletion in Nb-Ta (Fig. 8b), relatively high Sr isotopic composition and weak negative $\varepsilon_{Nd}(t)$ (−0.89 to −2.89; Table 4; Fig. 9), suggest a role for a continental component in the magma genesis of the studied volcanic rocks. Crustal assimilation can cause significant variations in Sr–Nd isotopes within a group of rocks, and produces a negative correlation between SiO_2 and $\varepsilon_{Nd}(t)$ values, as

Table 3 Trace element contents (ppm) of representative volcanic rocks, southern Qiangtang Terrane, Gerze, northern Tibet

Sample	OU-6 (RV*)	GBPG-1 (RV*)	OU-6 (MV*)	GBPG-1 (MV*)	NL1	NL2	NL3	NL4	NL5	NL6	NL7	NL8	NL9	NL10	NL11	NL12	NL13	NL14	NL15	YD1	YD2	YD3	YD4	YD5	YD6	YD7	YD8
Sc	22.1	13.9	23.0	13.8	9.62	9.82	9.73	9.26	10.4	9.62	10.4	10.6	9.64	10.5	9.94	8.23	9.26	8.94	8.16	8.76	8.58	12.5	13.3	12.8	13.1	13.3	12.6
V	129	96.5	123	96.0	76.5	88.4	75.3	71.4	66.8	71.2	75.4	75.9	80.5	83.2	83.3	78.5	63.4	64.5	75.4	77.4	71.6	146	145	149	154	139	132
Cr	70.8	181	70.5	179	19.2	58.4	79.4	62.6	68.5	68.7	68.4	68.5	65.3	70.4	66.4	71.5	57.5	85.4	82.6	112	92.4	13.3	14.6	14.8	13.5	9.26	8.34
Co	29.1	19.5	28.2	19.8	124	104	281	108	24.4	47.5	35.3	23.5	89.4	68.3	76.3	55.3	24.4	26.6	45.5	56.3	40.5	40.5	34.6	28.2	28.4	50.5	32.4
Ni	39.8	59.6	40.0	57.2	11.5	22.3	38.4	20.7	26.9	28.7	28.2	28.3	29.2	31.4	30.7	33.4	25.7	36.4	40.7	47.4	42.3	6.27	6.58	6.73	6.93	2.44	2.05
Ga	24.3	18.6	24.1	19.2	24.6	20.6	22.1	21.4	22.4	22.3	21.4	21.6	21.7	22.8	22.6	20.1	21.5	19.6	18.6	19.3	19.5	15.4	14.7	16.1	15.4	17.5	17.4
Rb	120	56.2	117	57.5	133	98.4	104	114	131	115	124	128	118	124	118	104	116	108	91.2	98.6	106	50.4	49.6	51.5	57.6	64.6	60.8
Sr	131	364	128	365	671	766	885	783	776	775	758	753	746	782	766	671	697	774	735	754	784	974	1035	708	914	1125	937
Y	27.4	18.0	27.2	19.3	16.4	15.3	13.7	13.2	14.3	14.4	14.7	14.8	13.5	15.3	14.6	11.8	14.3	14.3	13.1	13.3	13.6	14.3	14.8	15.2	14.3	21.3	22.6
Zr	174	232	169	251	292	275	269	272	283	286	294	296	275	293	284	273	296	284	276	271	276	274	266	278	264	285	288
Nb	14.8	9.9	14.7	10.1	18.4	16.7	15.6	14.6	15.1	16.2	17.2	17.5	17.6	17.4	18.1	16.5	18.3	19.4	17.1	17.2	17.4	16.6	15.9	17.6	15.6	17.6	18.3
Ba	477	908	480	915	828	847	864	824	875	822	834	842	817	856	843	783	806	1296	792	815	1236	546	442	527	585	762	995
La	33.0	53.0	32.6	54.0	68.3	67.2	66.4	63.4	67.6	66.4	67.9	67.8	65.4	70.2	67.2	60.5	66.6	66.5	60.5	61.2	61.4	62.5	62.4	61.6	62.7	61.6	62.1
Ce	74.4	103.2	79.1	94.7	134	135	127	123	124	126	121	126	125	135	131	124	121	125	123	106	105	108	95.5	105	113	106	96.3
Pr	7.80	11.5	7.71	12.0	13.8	13.5	13.2	12.7	13.2	13.3	13.4	13.2	12.8	13.7	13.3	11.8	13.3	13.2	12.4	10.6	10.8	9.34	9.26	9.74	9.62	10.9	11.2
Nd	29.0	43.3	29.9	44.2	46.5	47.6	45.4	43.4	46.3	46.1	48.2	45.8	44.5	48.5	46.6	41.7	46.2	47.3	42.7	31.6	31.8	28.2	26.8	28.5	27.4	29.2	28.6
Sm	5.92	6.79	5.79	7.06	6.68	7.14	6.78	6.36	7.05	6.85	7.33	7.06	6.68	6.91	6.85	6.38	7.18	7.08	6.64	6.63	7.16	5.43	5.36	5.58	5.45	5.65	5.59
Eu	1.36	1.79	1.34	1.82	1.65	1.81	1.72	1.55	1.73	1.65	1.63	1.69	1.71	1.68	1.66	1.53	1.56	1.69	1.61	1.46	1.45	1.04	1.02	1.05	1.03	1.38	1.55
Gd	5.27	4.74	5.20	4.89	4.55	4.88	4.84	4.45	4.71	4.82	4.64	4.91	4.95	4.88	4.65	4.78	5.28	5.76	5.25	5.43	5.78	3.24	3.11	3.36	3.18	5.07	5.52
Tb	0.85	0.60	0.84	0.65	0.64	0.65	0.63	0.58	0.58	0.63	0.62	0.63	0.62	0.62	0.61	0.62	0.67	0.68	0.66	0.68	0.69	0.46	0.47	0.49	0.46	0.73	0.78
Dy	4.99	3.26	4.98	3.33	2.81	2.95	2.83	2.63	2.76	2.83	2.85	2.78	2.74	2.81	2.83	2.43	2.86	2.84	2.59	2.69	2.82	2.52	2.52	2.61	2.41	3.72	4.15
Ho	1.01	0.69	1.04	0.67	0.52	0.54	0.52	0.45	0.47	0.48	0.51	0.52	0.51	0.51	0.52	0.42	0.48	0.48	0.45	0.46	0.49	0.49	0.51	0.52	0.49	0.74	0.79
Er	2.98	2.01	2.97	2.08	1.36	1.37	1.35	1.22	1.28	1.29	1.32	1.29	1.32	1.29	1.38	1.22	1.42	1.41	1.28	1.32	1.29	1.56	1.58	1.63	1.45	1.43	1.44
Tm	0.44	0.30	0.43	0.31	0.18	0.16	0.17	0.16	0.14	0.16	0.15	0.15	0.16	0.17	0.16	0.18	0.18	0.17	0.14	0.15	0.18	0.18	0.19	0.20	0.16	0.22	0.23
Yb	3.00	2.03	2.97	2.11	1.04	1.06	1.02	0.96	0.98	1.04	1.04	1.02	0.96	1.03	1.04	0.96	1.05	1.08	0.98	1.02	1.13	1.28	1.26	1.25	1.27	1.24	1.26
Lu	0.45	0.31	0.45	0.32	0.15	0.16	0.16	0.15	0.14	0.16	0.15	0.15	0.15	0.16	0.15	0.15	0.16	0.15	0.14	0.15	0.14	0.15	0.14	0.15	0.13	0.16	0.14
Hf	4.70	6.07	4.68	6.12	5.48	4.65	4.57	3.89	4.22	4.62	4.55	4.58	4.53	4.47	4.56	5.42	5.33	5.38	4.34	5.05	5.18	4.41	4.26	5.15	4.21	5.23	5.31
Ta	1.06	0.40	1.11	0.42	1.04	1.03	1.01	0.94	1.05	1.02	1.05	0.92	1.04	1.03	1.05	1.04	1.06	1.32	1.03	1.03	1.04	0.86	0.75	1.02	0.73	1.05	1.06
Pb	28.2	14.1	32.3	13.4	35.2	32.5	37.5	34.4	33.4	32.7	32.4	31.3	33.4	33.5	33.9	33.9	25.5	30.4	27.2	29.4	29.2	17.4	18.5	18.8	19.2	19.8	20.2
Th	11.5	11.2	11.2	12.0	18.6	14.2	15.5	16.6	17.3	16.5	16.3	16.1	16.4	16.8	16.2	15.2	15.3	14.7	14.6	15.3	15.3	4.85	4.65	5.04	4.63	9.65	9.74
U	1.96	0.90	1.97	0.91	2.93	2.25	4.33	4.24	2.69	2.62	2.56	2.54	2.59	2.69	2.68	2.47	2.42	2.41	2.53	2.39	2.58	1.21	1.25	1.33	1.22	2.38	2.34
$(La/Yb)_N$	7.9	18.7	7.9	18.4	47.1	45.5	46.7	47.4	49.5	45.8	46.8	47.7	48.9	48.9	46.3	45.2	45.5	44.2	44.3	43.0	39.0	35.0	35.5	35.3	35.4	35.6	35.4
Eu/Eu*	0.18	0.24	0.18	0.23	0.22	0.23	0.22	0.22	0.22	0.21	0.21	0.21	0.22	0.22	0.22	0.21	0.19	0.20	0.20	0.21	0.20	0.24	0.24	0.23	0.23	0.19	0.21

Continued Table 3

YD9	YD10	YD11	YD12	QG1	QG2	QG3	QG4	QG5	QG6	QG7	QG8	QG9	QG10	QG11	QG12	QG13	QG14	QG15	XB1	XB2	XB3	XB4	XB5	XB6	XB7	XB8	XB9	XB10	XB11	XB12
13.5	13.7	13.9	13.6	13.7	13.5	13.6	15.4	16.5	15.9	15.7	16.1	15.5	15.6	15.8	15.4	15.6	14.8	14.9	15.4	15.7	15.6	15.4	16.8	16.5	16.4	16.5	16.3	16.6	16.5	15.9
146	139	145	135	133	135	144	158	164	158	166	175	157	176	168	175	164	152	158	163	172	159	148	195	168	153	144	156	149	138	142
8.94	8.07	8.42	9.76	9.45	8.76	12.4	12.3	9.16	9.64	9.23	15.7	9.83	9.73	10.8	10.4	9.83	14.2	13.8	9.93	13.5	11.3	8.73	13.3	11.4	8.12	8.38	8.92	9.16	9.68	11.6
34.3	30.4	23.6	21.2	20.4	19.8	26.2	26.8	31.3	26.4	29.4	27.6	26.5	27.3	37.8	39.5	38.3	40.3	37.6	32.5	41.8	32.4	25.3	54.5	40.5	21.8	21.2	23.4	41.8	33.3	29.4
3.06	2.54	2.43	3.57	1.71	1.94	2.97	4.65	2.17	2.53	2.47	6.15	2.92	2.36	3.35	2.94	3.46	5.24	2.96	4.62	6.03	2.73	3.35	4.92	3.05	3.48	3.04	2.64	2.96	3.38	5.33
17.8	18.1	17.1	16.8	17.3	17.3	17.3	18.7	19.2	18.2	19.6	19.3	19.4	20.1	20.1	20.2	19.8	19.6	19.5	19.8	20.2	20.4	19.6	24.3	19.4	18.8	19.1	17.8	19.3	18.9	18.6
70.9	86.6	74.5	75.4	81.4	80.4	73.8	80.7	76.3	74.3	74.3	74.5	72.2	76.2	72.4	76.5	72.8	81.5	76.4	74.6	67.4	79.2	85.8	125	96.1	79.6	72.6	80.4	75.6	73.8	65.5
967	831	893	796	784	775	986	942	1224	1229	1337	1231	1428	1406	1124	1006	992	984	928	1432	1224	1336	1235	1341	1249	1326	1325	1243	1323	1263	1125
23.4	21.5	21.6	22.3	21.6	21.2	22.5	23.2	24.5	23.5	23.7	23.8	24.6	24.6	24.5	25.3	25.2	25.2	25.2	25.2	24.8	25.2	24.2	30.2	24.2	24.5	23.5	23.4	22.8	22.6	24.3
294	275	266	263	143	146	147	152	162	166	168	175	167	173	178	171	164	167	174	158	162	165	166	184	175	176	165	175	179	174	179
18.6	17.4	14.8	15.1	11.2	11.4	11.3	10.4	12.1	11.6	11.8	12.2	11.3	11.7	12.4	11.4	11.1	11.3	12.2	10.8	11.2	11.4	11.3	12.5	12.1	12.2	11.1	12.2	12.4	10.9	12.3
865	784	1642	1361	1342	1216	1159	868	983	843	594	595	608	617	636	635	605	587	592	638	598	634	654	838	622	737	682	729	636	628	814
62.6	62.7	62.8	62.3	62.5	62.3	61.8	62.3	62.5	61.4	62.3	62.5	61.6	62.4	62.6	62.5	62.7	62.3	62.5	63.3	62.8	62.7	62.5	63.4	62.3	62.7	63.1	63.5	62.8	62.7	63.4
103	107	105	106	113	114	116	117	115	113	114	118	115	114	115	113	115	114	113	118	119	121	118	121	119	117	116	116	117	118	119
11.4	11.3	11.5	10.5	9.86	10.8	11.3	11.5	11.2	10.6	10.9	10.7	11.2	11.3	11.2	11.5	11.4	11.5	11.2	12.4	12.2	12.3	12.2	12.5	12.2	12.3	11.8	11.9	11.6	11.8	11.4
29.3	28.6	28.5	27.2	26.2	26.8	28.8	28.6	30.4	29.2	30.6	30.2	31.3	30.5	31.3	31.8	31.8	31.8	30.6	31.3	30.6	31.8	31.3	37.8	30.3	30.8	28.8	29.3	29.2	30.2	30.2
5.64	5.62	5.45	5.33	5.21	5.06	5.65	5.41	5.75	5.55	5.71	5.68	5.89	6.02	6.08	6.18	6.16	6.04	5.84	6.03	5.98	5.96	6.05	7.33	5.86	5.95	5.55	5.76	5.62	5.83	6.04
1.59	1.44	1.52	1.38	1.48	1.33	1.51	1.42	1.53	1.51	1.54	1.45	1.52	1.52	1.59	1.63	1.58	1.53	1.58	1.61	1.56	1.58	1.48	1.88	1.52	1.54	1.38	1.43	1.53	1.46	1.63
5.46	5.09	5.39	5.24	5.23	4.95	5.45	5.15	5.54	5.17	5.35	5.14	5.23	5.43	5.38	5.48	5.66	5.56	5.61	5.32	5.25	5.42	5.53	5.58	5.21	5.62	5.08	5.15	5.13	5.19	5.34
0.79	0.73	0.75	0.75	0.72	0.72	0.72	0.76	0.79	0.78	0.78	0.78	0.83	0.82	0.79	0.85	0.83	0.82	0.82	0.83	0.82	0.82	0.82	0.84	0.82	0.79	0.75	0.74	0.74	0.76	0.78
4.13	3.84	3.84	3.95	3.86	3.71	3.89	3.98	4.18	4.04	4.06	4.04	4.11	4.24	4.25	4.24	4.26	4.28	4.28	4.42	4.16	4.19	4.04	4.04	4.06	4.15	4.02	3.92	3.93	4.03	4.16
0.78	0.75	0.78	0.78	0.75	0.72	0.75	0.78	0.83	0.82	0.82	0.81	0.82	0.85	0.85	0.88	0.84	0.85	0.87	0.86	0.83	0.83	0.82	0.85	0.81	0.82	0.82	0.78	0.75	0.75	0.82
1.43	1.42	1.43	1.43	1.41	1.42	1.39	1.42	1.43	1.38	1.35	1.34	1.34	1.42	1.43	1.43	1.42	1.43	1.43	1.42	1.42	1.41	1.38	1.44	1.41	1.42	1.42	1.37	1.36	1.36	1.41
0.22	0.21	0.22	0.23	0.21	0.21	0.16	0.22	0.22	0.21	0.23	0.22	0.21	0.23	0.22	0.22	0.21	0.22	0.21	0.22	0.21	0.21	0.22	0.23	0.22	0.21	0.22	0.21	0.22	0.21	0.22
1.27	1.29	1.28	1.25	1.23	1.24	1.26	1.28	1.24	1.25	1.25	1.23	1.23	1.24	1.24	1.23	1.24	1.24	1.23	1.25	1.24	1.23	1.24	1.26	1.23	1.24	1.27	1.28	1.24	1.25	1.26
0.16	0.14	0.13	0.16	0.13	0.13	0.14	0.13	0.16	0.14	0.15	0.15	0.15	0.16	0.16	0.15	0.14	0.14	0.16	0.15	0.15	0.15	0.14	0.16	0.15	0.15	0.13	0.15	0.14	0.15	0.15
5.42	4.32	4.16	4.06	3.12	3.61	3.73	3.52	3.44	3.55	3.67	3.82	3.38	3.94	3.95	3.84	3.69	3.71	3.64	3.43	3.52	3.61	3.46	3.83	3.58	3.46	3.48	3.63	3.65	3.36	3.41
1.08	0.85	0.71	0.65	0.73	0.66	0.64	0.68	0.45	0.71	0.74	0.86	0.67	0.91	0.81	0.83	0.78	0.65	0.73	0.69	0.72	0.83	0.75	0.84	0.66	0.59	0.75	0.83	0.85	0.45	0.56
24.8	22.5	25.5	22.4	23.3	21.7	19.2	22.4	19.7	17.8	29.2	23.8	19.1	20.8	17.5	18.4	19.6	24.5	23.6	20.5	20.3	19.4	17.1	29.6	22.3	17.3	21.8	18.6	15.1	17.6	24.3
9.83	9.74	9.43	9.65	9.38	9.48	9.64	10.5	10.4	9.94	10.3	10.5	10.2	10.5	10.8	10.8	10.6	10.3	10.6	10.3	10.2	10.5	10.2	13.3	10.2	10.4	10.3	10.3	9.96	10.2	10.4
2.05	2.35	2.43	2.34	2.33	2.23	2.17	2.02	2.23	1.94	2.19	2.24	2.18	2.26	2.36	2.36	2.25	2.28	2.25	2.32	2.18	2.12	2.03	2.72	1.89	2.38	2.12	2.33	2.25	2.32	2.14
35.4	34.9	35.2	35.8	36.4	36.0	35.2	34.9	36.2	35.2	35.8	36.4	35.9	36.1	36.2	36.4	36.3	36.0	36.4	36.3	36.3	36.6	36.2	36.1	36.3	36.3	35.6	35.6	36.3	36.0	36.1
0.21	0.20	0.21	0.20	0.21	0.20	0.20	0.20	0.20	0.21	0.21	0.20	0.20	0.20	0.21	0.21	0.20	0.20	0.21	0.21	0.21	0.21	0.19	0.20	0.21	0.20	0.19	0.20	0.21	0.20	0.21

RV*: recommended values; MV*: measured values. Values for OU–6 are from Potts and Kane (2005).

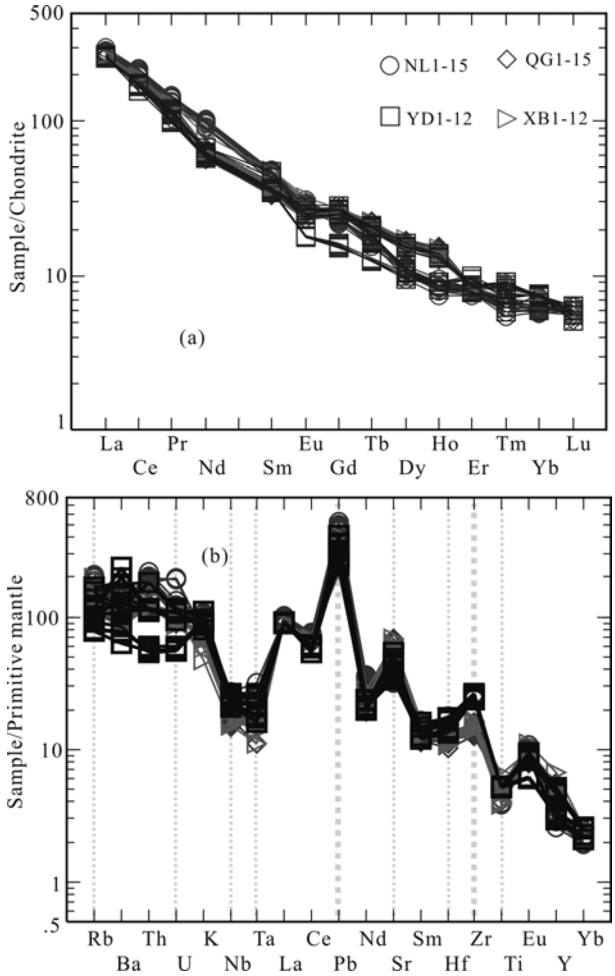

Fig. 8. (a), Chondrite-normalized rare earth element patterns and (b), primitive mantle-normalized spider diagrams for the volcanic rocks of the southern Qiangtang Terrane study area, Gerze, northern Tibet.

Primitive mantle and chondritic abundances were taken from Sun and McDonough (1989).

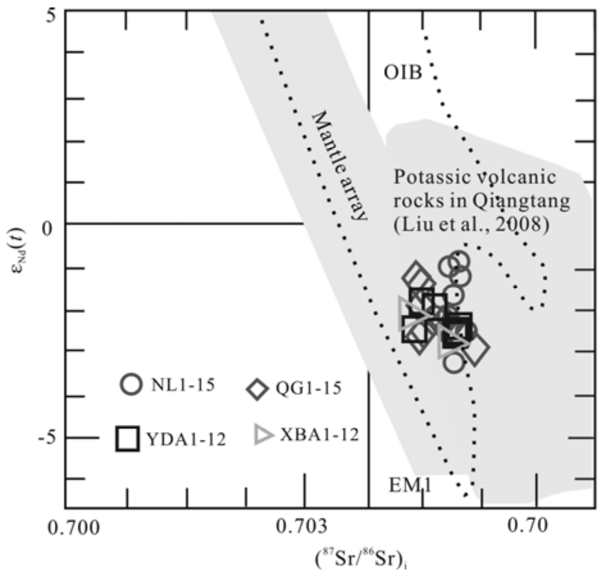

Fig. 9. Plot of $(^{87}Sr/^{86}Sr)_i$ vs. $\varepsilon_{Nd}(t)$ for the volcanic rocks from the southern Qiangtang Terrane study area, Gerze, northern Tibet.

well as a positive correlation between SiO_2 and $(^{87}Sr/^{86}Sr)_i$ values. These features, however, are not observed in the volcanic rocks studied from Nile, Yaduo, Quegang, and Xiuba counties, indicating a general lack of crustal contamination in Gerze area volcanism (Fig. 11a, b). This is supported also by other geochemical evidence, i.e., Ce vs. Ce/Yb, and Eu/Yb vs. La/Yb related diagrams (Fig. 12a, b). In addition, the studied volcanic rocks are characterized by relatively low contents of Nb (10.4–19.4 ppm), Zr (in more than half of the samples this is <180 ppm), Th (<16.0 ppm except for a few samples), and Rb (<80 ppm for most samples) (Table 3), when compared to the upper crust (which yields typical values of Nb=25 ppm, Zr=190 ppm, Th=10.5 ppm, and Rb=84 ppm; Rudnick and Fountain, 1995; Rudnick and Gao, 2003), also suggestive of negligible crustal contamination. Moreover, the studied volcanic rocks are characterized by relatively low U (<2.4 ppm except for a few samples) compared to the upper crust (e.g., U=2.7 ppm, Rudnick and Fountain, 1995; Rudnick and Gao, 2003), further suggesting that crustal contamination was insignificant. In summary, we propose that the geochemical and Sr–Nd isotopic signatures of the volcanic rocks studied are inherited mainly from the source prior to emplacement and do not reflect significant crustal assimilation.

5.3 Genetic model

The closure of the Banggongco–Nujiang Ocean resulted in collision and amalgamation of the Qiangtang and Lhasa Terranes (Zhang et al., 2006a, b). During the Berriasian–Valanginian period of the Early Cretaceous, uplift of the Qiangtang Terrane led to the development of the Banggongco–Nujiang Suture, and mylonite generated covered extensive areas along its margin with the Lhasa Terrane (Wang Yang, 2007). Subsequently, post-arc extension occurred in the northern Lhasa Terrane and southern Qiangtang Terrane, during the Hauterivian–lower Barremian period, in response to the rollback of the Neo-Tethys oceanic crust. Thereafter, large scale continental rifting and the eruption of basalt appeared adjacent to Banggongco–Nujiang Suture, as well as the emplacement of extensive intermediate–felsic and bimodal volcanic rocks, along the northern margin of the Lhasa Terrane and other regions (Wang Yang, 2007). Generally, there are three genetic models to account for the origin of the intermediate volcanic rocks in our study area: (1) fractional crystallization of a basaltic magma, because these rocks may occur together with intermediate–felsic magmas, and have similar Sr isotopic compositions; (2) combined magma assimilation and AFC and (3) partial

Table 4 Sr–Nd isotopic compositions for volcanic rocks in Gerze, southern Qiangtang Terrane, northern Tibet

Sample	Sm (ppm)	Nd (ppm)	Rb (ppm)	Sr (ppm)	$^{87}Rb/^{86}Sr$	$^{87}Sr/^{86}Sr$	2δ	$(^{87}Sr/^{86}Sr)_i$	$^{147}Sm/^{144}Nd$	$^{143}Nd/^{144}Nd$	2δ	$(^{143}Nd/^{144}Nd)i$	$\varepsilon_{Nd}(t)$
NL1	3.37	17.2	48.5	1283	0.1095	0.705672	12	0.705480	0.1184	0.512502	9	0.512407	−1.42
NL2	5.59	29.2	61.3	925	0.1919	0.705893	13	0.705557	0.1157	0.512403	10	0.512310	−3.31
NL3	4.46	28.6	75.2	876	0.2486	0.706114	14	0.705679	0.0943	0.512423	10	0.512346	−2.57
NL5	5.22	26.3	81.3	769	0.3061	0.706085	13	0.705543	0.1200	0.512494	8	0.512396	−1.59
NL6	5.56	29.4	73.8	1195	0.1788	0.705964	14	0.705616	0.1143	0.512508	8	0.512415	−1.23
NL8	5.74	30.7	73.6	1266	0.1683	0.705914	11	0.705625	0.1130	0.512524	12	0.512432	−0.89
NL9	6.05	30.7	76.4	1294	0.1710	0.705928	12	0.705474	0.1191	0.512523	10	0.512427	−1.02
NL11	6.08	31.4	71.5	1035	0.2000	0.705825	13	0.705474	0.1170	0.512457	10	0.512362	−2.28
NL12	6.05	31.8	81.5	981	0.2406	0.705695	12	0.705272	0.1150	0.512455	10	0.512362	−2.28
NL15	6.04	31.7	79.4	1291	0.1781	0.705914	13	0.705601	0.1152	0.512443	9	0.512350	−2.52
YD1	5.55	29.2	72.6	1195	0.1759	0.705876	12	0.705567	0.1149	0.512441	9	0.512348	−2.55
YD2	5.78	30.3	70.7	1306	0.1568	0.705868	14	0.705593	0.1153	0.512448	9	0.512355	−2.42
YD5	3.56	17.4	29.3	1034	0.0821	0.705423	13	0.705279	0.1237	0.512478	8	0.512378	−1.97
YD6	3.64	19.4	45.4	1447	0.0909	0.705692	12	0.705088	0.1134	0.512476	10	0.512384	−1.85
YD10	4.14	20.6	32.5	426	0.2209	0.705476	14	0.704962	0.1215	0.51245	9	0.512352	−2.48
QG2	4.03	20.4	32.3	405	0.2309	0.705367	12	0.705051	0.1194	0.512482	9	0.512386	−1.83
QG4	4.27	21.3	96.4	522	0.5347	0.705988	10	0.705051	0.1212	0.512443	9	0.512345	−2.62
QG5	4.43	21.6	49.5	508	0.2822	0.705617	14	0.705123	0.1240	0.512454	7	0.512354	−2.45
QG7	5.24	26.7	42.3	713	0.1718	0.705313	13	0.705012	0.1186	0.512513	10	0.512417	−1.21
QG8	5.63	30.5	53.4	827	0.1870	0.705349	13	0.705021	0.1116	0.512498	12	0.512408	−1.39
QG12	5.76	30.6	74.5	1316	0.1639	0.706114	12	0.705827	0.1138	0.512423	10	0.512331	−2.89
XB2	3.55	16.8	46.7	1533	0.0882	0.705087	14	0.704932	0.1277	0.512476	10	0.512373	−2.08
XB3	5.45	27.6	72.8	1242	0.1697	0.705876	13	0.705500	0.1194	0.512443	10	0.512347	−2.59
XB7	5.83	31.3	71.3	982	0.2102	0.705868	12	0.705660	0.1126	0.512441	8	0.512350	−2.52
XB9	5.46	28.5	73.4	1225	0.1735	0.705964	13	0.705505	0.1158	0.512507	10	0.512414	−1.28
XB10	5.44	28.2	58.6	766	0.2215	0.705893	14	0.705505	0.1166	0.512504	9	0.512504	−2.61

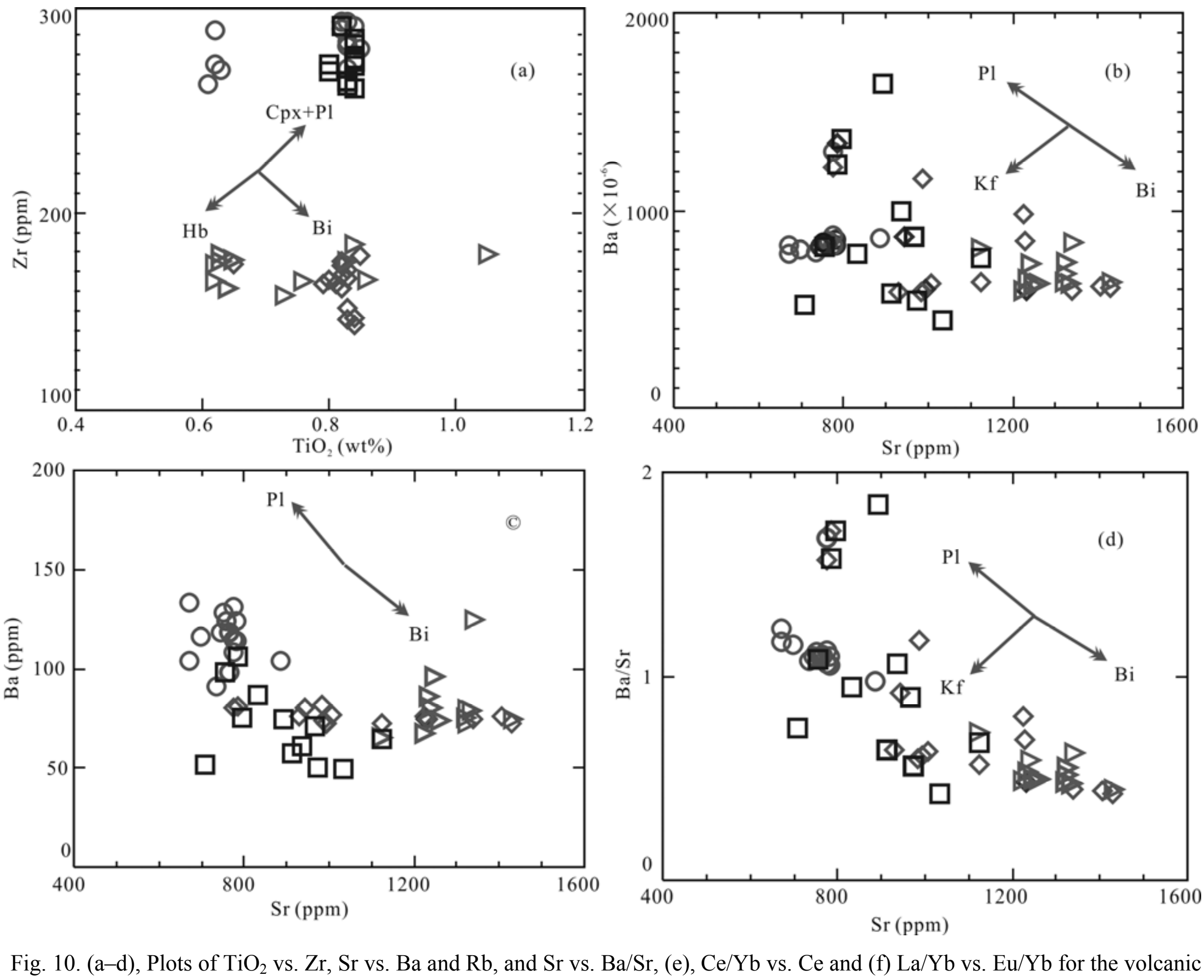

Fig. 10. (a–d), Plots of TiO_2 vs. Zr, Sr vs. Ba and Rb, and Sr vs. Ba/Sr, (e), Ce/Yb vs. Ce and (f) La/Yb vs. Eu/Yb for the volcanic rocks from the southern Qiangtang Terrane study area, Gerze, northern Tibet.

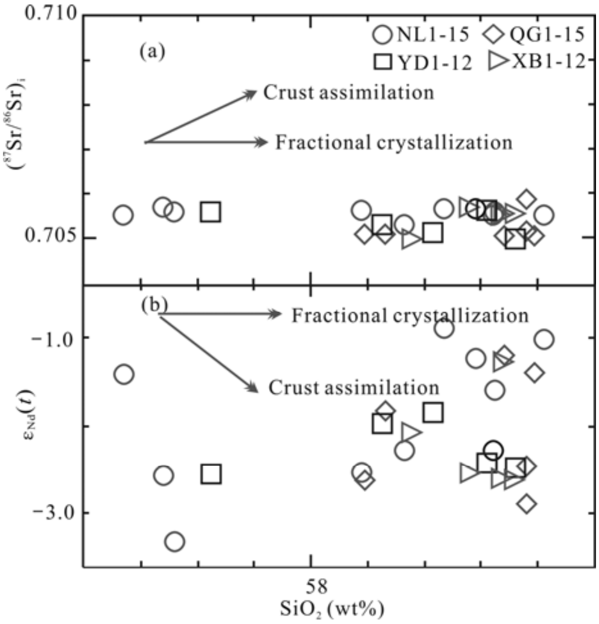

Fig. 11. Plots of the initial $^{87}Sr/^{86}Sr$ ratio (a) and $\varepsilon_{Nd}(t)$ vs. SiO_2 (%)(b) for the investigated volcanic rocks from the study area, southern Qiangtang Terrane, Gerze, northern Tibet, indicating crystal fractionation to be the dominant control in their evolution.

FC, fractional crystallization; AFC, assimilation and fractional crystallization.

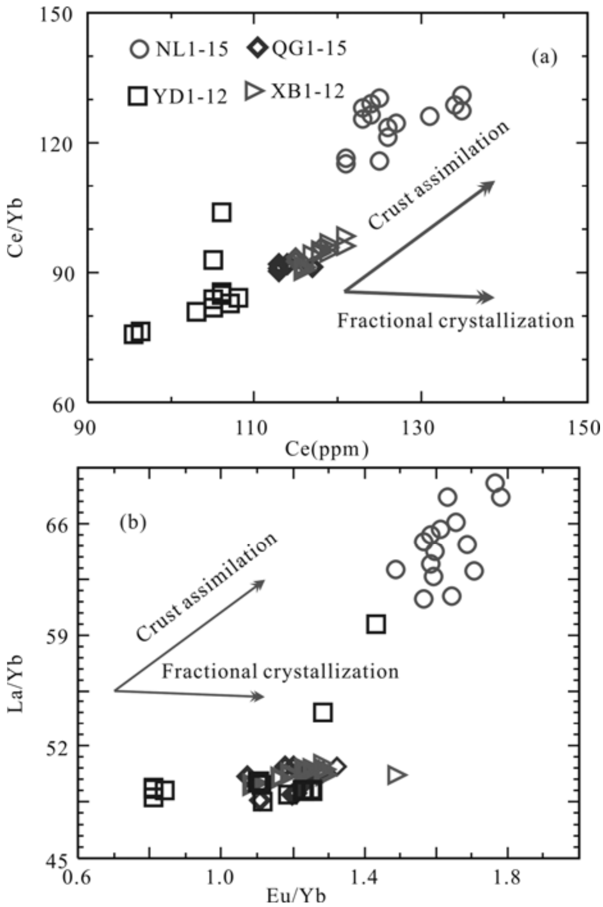

Fig. 12. Plots of Ce vs. Ce/Yb (a) and Eu/Yb vs. La/Yb (b) related diagrams for the investigated volcanic rocks from the study area, southern Qiangtang Terrane, Gerze, northern Tibet.

melting of crustal rocks at depth, possibly as a result of underplating (Zhu et al., 2006).

In this section, we aim to address the origins of the investigated Gerze volcanic rocks in relation to the above models. The geochemical and isotopic evidence presented earlier does not support crustal involvement in the origin of these rocks. Thus, we can preclude genetic model 2. Model 3 is a widely accepted genetic model for the generation of intermediate–felsic volcanic rocks at a destructive plate margin (e.g., Hawkesworth et al., 1994). We have shown that the investigated volcanic rocks are not products of crustal melting; thus, this model is also unlikely. On the basis of our data it is necessary, therefore, to evaluate and discuss the likelihood of the first model in accounting for the generation of Gerze area volcanic rocks. The results of our studies indicate that the geochemical and isotopic features of the studied volcanic rocks reflect that of a heterogeneous mantle source. Furthermore, there is clear evidence in favour of fractional crystallization having affected the parental magmas to the Gerze volcanic rocks, likely to have occurred during magma ascent; in other words, these volcanic rocks were derived from a parental magma more mafic than andesite (e.g., basalt or a “primitive or primary” andesite). The fact that there are no basaltic rocks observed in the study area, might suggest that fractional crystallization of any basalt magma could have occurred at depth (i.e., the basalts could have arrested their ascent in crustal rocks below the current level of erosion, or these may indeed have pounded at the base of the crust). In other words, the parental basaltic magma to the studied rocks was not erupted at or near surface. An alternative explanation is that all of the basalt rocks in the study area have been removed by erosion. This seems unlikely, and based upon our discussion above, we favor that the Gerze area volcanic rocks derive by means of model 1; that is, and these represent the products of fractional crystallization of a parental, basaltic magma. Accordingly, we envisage that during the Late Triassic (140 Ma), collision of the Lhasa Terrane and Qiangtang Terrane occurred due to the subduction of the Banggongco-Nujiang ocean (Fig. 13a), resulting in lithospheric thickening, as exemplified in the significant quantities of ancient metamorphic rocks identified in the central Qiangtang Terrane. From Late Triassic to early Jurassic times, the Qiangtang Terrane was characterized by oceanic lithosphere break–off, high– to ultra–high-pressure metamorphism and denudation, and regional-scale extension (Fig. 13b). Subsequently, during the early Cretaceous partial melting of a heterogeneous

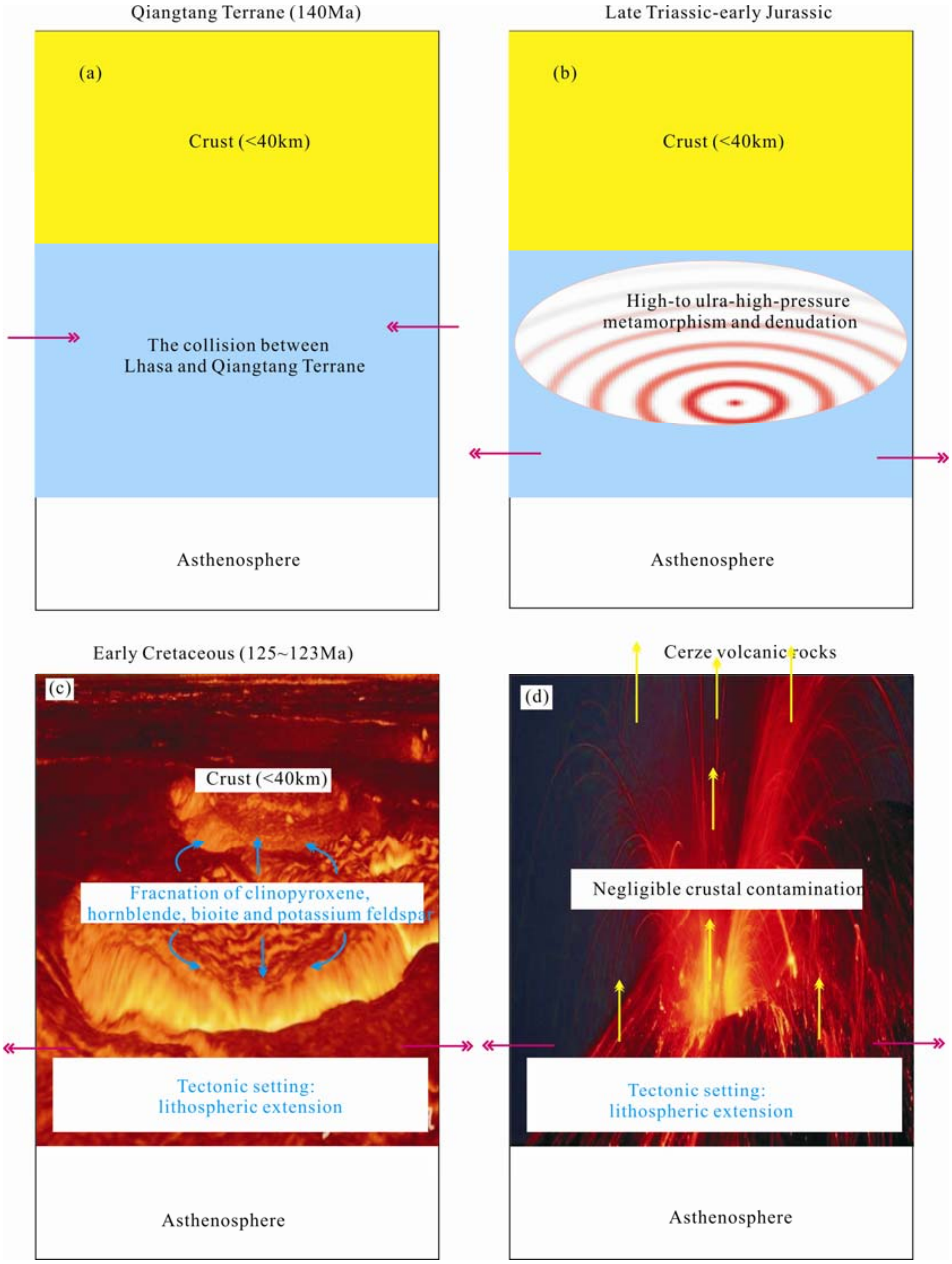

Fig. 13. Diagram illustrating tectonic evolution in northern Tibet.
(a), 140 Ma: collision of the Lhasa Terrane and Qiangtang Terrane resulted in thick lithosphere (mantle and lower crust); (b), Late Triassic to early Jurassic: high– to ultra–high pressure and lithospheric extension occurred; (c), 125–123 Ma: primitive magma appeared due to decompressional melting, after fractionation of clinopyroxene, hornble, biotite, and potassium feldspar during magma emplacement, meanwhile, however, (d), negligible crustal contamination occurred before the studied volcanic rocks occurrence in Gerze, northern Tibet.

mantle source below the study area, led to the formation and ascent of basaltic parental magmas to the Gerze region volcanic rocks, that gained their intermediate compositions chiefly through the fractional crystallization of clinopyroxene, hornblende, biotite, and potassium feldspar, during ascent of these magmas prior to their eruption between 123–125 Ma, however, negligible crustal contamination occurred during magma ascent (Fig. 13c, d).

6 Conclusions

New geochronological, geochemical, and Sr–Nd isotopic data for the studied Gerze region volcanic rocks allow us to reach the following conclusions:

(1) LA-ICP-MS U-Pb zircon age data indicate that the volcanic rocks were formed between 123.1±0.94 Ma and 124.5±0.89 Ma, i.e., during the Early Cretaceous.

(2) The volcanic rocks belong to the alkaline and sub–alkaline magma series, and show both calc–alkaline and shoshonitic affinities, as indicated by their K_2O and Na_2O contents. The rocks are enriched in light rare earth elements [$(La/Yb)_N$=34.9–49.5)] and large-ion lithophile elements (e.g., Rb, Ba, Th, U, K, Pb and Sr), and show slightly negative Eu anomalies (Eu/Eu*=0.19–0.24) and negative anomalies in high field strength elements (Nb, Ta, Hf, and Ti), relative to primitive mantle. These geochemical signatures are typical of magmas formed in a destructive plate-margin setting, or from a source that inherited such geochemical characteristics during an earlier episode of subduction. The calculated zircon saturation temperatures (tZr°C) of the volcanic rocks range from 783 to 874°C.

(3) The volcanic rocks derived from a compositionally heterogeneous mantle source, and through fractional crystallization of a basaltic parental magma. Fractionation (involving clinopyroxene, hornblende, biotite, potassium feldspar) occurred during ascent of these volcanic rocks, with negligible crustal contamination.

Acknowledgments

The authors thank Dr. Shuqin Yang for his assistance during the XRF analyses, Professor Liang Qi and Ms. Jing Hu for their assistance with the ICP-MS analyses, the analysts for their assistance during TIMS Sr-Nd isotopic analyses, and Professors Xiaoming Li and Honglin Yuan for their assistance during LA-ICP-MS U-Pb dating and Hf isotopic analyses. This study was supported by the National Natural Science Foundation of China (grants # 41373028 and 41573022).

Manuscript received Jan. 21, 2018
Accepted Aug. 10, 2018
edited by Fei Hongcai

References

Allègre, C.J., Courtillot, V., Tapponnier, P., Hirn, A., Mattauer, M., Coulon, C., Jaeger, J.J., Achache, J., Schärer, U., Marcoux, J., Burg, J.P., Girardeau, J., Gariépy, C., Gopel, C., Li, T.D., Xiao, X.C., Chang, C.F., Li, G.G., Lin, B.Y., Teng, J.W., Wang, N.W., Chen, G.M., Han, T.L., Wang, X.B., Sheng, H.B., Cao, Y.Q., Zhou, J., Giu, H.R., Bao, P.S., Wang, S.C., Wang, B.X., Zhou, Y.X., and Ronghua, X., 1984. Structure and evolution of the Himalaya-Tibet orogenic belt. *Nature*, 307: 17–22.

Andersen, T., 2002. Correction of common lead in U-Pb analyses that do not report ^{204}Pb. *Chemical Geology*, 192: 59–79.

Bureau of Geology and Mineral Resources of Tibet Autonomous Region (BGMRTAR), 1993. *Bureau of Geology and mineral resources of Tibet Autonomous Region*. Beijing: Geological Publishing House, 406–408.

Burg, J.P., Chen and G.M., 1984. Tectonic and structureal zonation of southern Tibet, China. *Nature*, 311: 219–223.

Chang, C.F., Chen, N. S., Coward, M.P., Deng, W.M., Dewey, J.F., Gansser, A., Narris, N.B.W., Jin, C.W., Kidd, W.S.F., Leeder, M.R., Li, H., Lin, J.L., Liu, C.J., Mei, H.J., Molnar, P., Pan, Y., Pan, Y.S., Pearce, J.A., Shackleton, R.M., Smith, A.B., Sun, Y.Y., Ward, M., Watts, D.R., Xu, J.T., Xu, R.H., Yin, J.X. and Zhang, Y.Q., 1986. Preliminary conclusions of The Royal Society / Academia Sinica 1985 Geotraverse of Tibet. *Nature*, 323: 501–507.

Chi Xiaoguo, Li Cai and Jin Wei, 2005. Cenozoic volcanism and tectonic evolution of lithosphere in Qiangtang, northern Tibet. *Science in China*, 35(7): 399–401.

Chung, S.L., Zhang, Y.Q., Xie, Y.W., Lo, C.H., Chu, M.F., Lee, T.Y., Li, X.H., Zhang, Q., and Wang, Y.Z., 2005. Tibetan tectonic evolution inferred from spatial and temporal variations in Post-collisional magmatism. *Earth-Science Reviews*, 68: 173–196.

Deng Wanming, 1989. The Cenozoic volcanic in north Ali area, Xizang. *Acta Petrologica Sinica*, 5(3): 1–11 (in Chinese with English abstract).

Deng Wanming, 1998. *Cenozoic intraplate volcanic rocks in the northern Qinghai-Xizang plateau*. Beijing: Geological Publishing House, 1–178.

Deng Wanming, 1999. The geology, geochemistry and forming age of the shoshonitic volcanic rocks in middle Kunlun orogenic belt. *Scientia Geologica Sinica,* 3: 201–213 (in Chinese with English abstract).

Dewey, J.F., Shackleton, R.M., Chang, C., and Sun, Y.Y., 1988. The tectonic development of the Tibet plateau. Philosophical Transactions of the Royal Society A: Mathematical, Physical and Engineering. *Sciences*, 327: 379–413.

Ding, L., Kapp, P., Yue, Y.H., and Lai, Q.Z., 2007. Post collisional calc-alkaline lavas and xenoliths from the southern Qiangtang Terrane, central Tibet. *Earth and Planetary Science Letters*, 255: 28–38.

Ding, L., Kapp, P., Zhong, D., and Deng, W., 2003. Cenozoic volcanism in Tibet: evidence for a transition from oceanic to continental subduction. *Journal of Petrology*, 44: 1833–1865.

Ding, L., Zhang, J.J., Zhou, Y., Deng, W.M., Xu, R.H., and Zhong, D.L., 1999. Tectonic implication on the lithosphere evolution of the Tibet plateau: petrology and northern Tibet. *Acta Petrogica Sinica*, 15(3): 408–421(in Chinese with English abstract).

England, P., and Houseman, G., 1986. Finite strain calculations of continental deformation: comparison with the India-Asia collision zone. *Journal of Geophysical Research*, 91: 3664–3676.

Girardeau, J., Marcoux, J., Bassoullet, J.P., Tang, Y.K., Xiao, X.C., Zao, Y.G., and Wang, X.B., 1984. Tectonic environment and geodynamic significance of the Neo-Cimmerian Dongqiao ophiolite, Bangong-Nujiang suture zone, Tibet.

Nature, 307: 27–31.

Girardeau, J., Marcoux, J., Fourcade, E., Bassoullet, J.P., and Tang, Y.K., 1985. Xainxa ultramafic rocks, central Tibet, China: Tectonic environment and geodynamic significance. *Geology*, 13: 330–333.

Guo, Z.F., Wilson, M., Liu, J.Q., and Mao, Q.A., 2006. Post-collisional potassic and ultrapotassic magmatism of the northern Tibetan plateau: constraints on characteristics of the mantle source, geodynamic setting and uplift mechanisms. *Journal of Petrology,* 47: 1177–1220.

Guynn, J.H., Kapp, P.P., Pullen, A., Heizler, M., Gehrels, G., and Ding, L., 2006. Tibetan basement rocks near Amdo reveal "missing" Mesozoic tectonism along the Bangong suture, central Tibet. *Geology*, 34: 505–508.

Hawkesworth, C.J., Gallagher, K., Hergt, J.M., and McDermott, F., 1994. Destructive plate margin magmatism: Geochemistry and melt generation. *Lithos*, 33: 169–188.

Kapp, P., Yin, A., Manning, C.E., Harrison, T.M., and Taylor, M.H., 2003. Tectonic evolution of the early Mesozoic blueschist-bearing Qiangtang metamorphic belt, central Tibet. *Tectonics*, 22: 1043.

Lai Shaocong and Liu Chiyang, 2001. Enriched upper mantle and eclogitic lower crust in north Qiangtang, Qinghai-Tibet Plateau: petrological and geochemical evidence from the Cenozoic volcanic rocks. *Acta Petrologica Sinica,* 17(3): 459–68 (in Chinese with English abstract).

Lai, S.M., Yang, J.S., Yildirim, D, M Xiong, F.H., and Chen, Y.H., 2018. Petrological and Os Isotopic Characteristics of Zedong Peridotites in the Eastern Yarlung–Zangbo Suture in Tibet. *Acta Geologica Sinica* (English Edition), 92(2): 442–461.

Leeder, M.R., Smith, A.B., and Yin, J., 1988. Sedimentology, palaeoecology and palaeo-environmental evolution of the 1985 Lhasa to Golmud Geotraverse. Philosophical Transactions of the Royal Society A: Mathematical. *Physical and Engineering Sciences*, 327: 107–143.

Li Cai, Cheng Liren and Hu Ke, 1995. *Investigation on the Longmucuo-Shuanghu ancient Tethys suture*. Geological Publishing House, 90–91 (in Chinese with English abstract).

Li Cai, Huang Xiaopeng, Mou Shiyong and Chi Xiaoguo, 2006. ^{40}Ar-^{39}Ar dating for Kangtog formation volcanic rocks in Zougouyouchaco, Qiangtang, northern Tibet. *Geological Bulletin of China,* 25(1): 226–8 (in Chinese with English abstract).

Li Cai, Wang Taiwu, Yang Deming and Yang Rihong, 2001. The lithological composition and tectonic evolution of central uplift, Qiangtang. *Journal of Changchun University of Science and Technology,* 31(1): 25–36 (in Chinese with English abstract).

Li, X.H., Li, Z.X., Li, W.X., Liu, Y., Yuan, C., Wei, G.J., and Qi, C.S., 2007. U-Pb zircon, geochemical and Sr-Nd-Hf isotopic constraints on age and origin of Jurassic I- and A-type granites from central Guangdong, SE China: a major igneous event in response to foundering of a subducted flat-slab? *Lithos,* 96: 186–204.

Liu Shen, Hu Ruizhong, Chi Xiaoguo, Li Cai and Feng Caixia, 2003. Geochemistry, series subdivision and petrogenetic interpretation of Cenozoic volcanic rocks in northern Tibet. *Geological Journal of China University*, 9(2): 279–292.

Liu, S., Hu, R.Z., Feng, C. X., Zou, H.B., Chi, X.G., Peng, J.T., Zhong, H., Qi, L., Qi, Y.Q., and Wang, T., 2008. Cenozoic high Sr/Y volcanic rocks in the Qiangtang Terrane, northern Tibet: geochemical and isotopic evidence for the origin of delaminated lower continental melts. *Geological Magazine*, 145: 463–474.

Liu, Y.S., Hu, Z.C., Zong, K.Q., Gao, C.G., Gao, S., Xu, J., and Chen, H.H., 2010. Reappraisement and refinement of zircon U -Pb isotope and trace element analyses by LA-ICP-MS. *Chinese Science Bulletin*, 55: 1535–1546.

Ludwig, K.R., 2003. User's manual for Isoplot/Ex, Version 3.00. A geochronological Toolkit for Microsoft Excel. *Berkeley Geochronology Center Special Publication*, 4: 1–70.

Miller, C., Sehuster, R., Klotzli, U., Mair, V.,Frank, W., and Purtseheller, F., 1999. Postcollisional Potassic and ultraPotassic magmatism in SW Tibet: geochemical and Sr-Nd-Pb-0 isotopic constrains for mantle sources characteristics and petrogenesis. *Journal of Petrology,* 4: 1399–1424.

Pan Rong, Zhu Xiaomin, Sun Chunqian, Wang Hao and Wang Hui, 2013. Pedefinition and geochemical characteristics of the Mesozoic shoshonite rock series of the Meifeng Formation in northern Yichun city, Heilongjiang province. *Geological Journal of China Universities*, 19(2): 316–326 (in Chinese with English abstract).

Pearce, J.A., and Deng, W.M., 1988. The ophioltes of the Tibet a geotraverse, Lhasa-Golmud (1985) and Lhasa to Kathmandu (1986). Philosophical Transactions of the Royal Society A: Mathematical. *Physical and Engineering Sciences*, 327: 215–238.

Potts, P.J., and Kane, J.S., 2005. International association of geoanalysts certificate of analysis: certified reference mantial OU-6 (penrhyn slate). *Geostandards and Geoanalytical Research*, 29: 233–236.

Qi, L., Hu, J., and Grégoire, D.C., 2000. Determination of trace elements in granites by inductively coupled plasma mass spectrometry. *Talanta,* 51: 507–513.

Sichuan Bureau of Geology and Mineral Resource (SBGMR), 1991. *Regional geology of Sichuan Province*. Beijing: Geological Publishing House.

Rowley, D.B., 1996. Age of initiation of collision between India and Asia: a review of stratigraphic data. *Earth and Planetary Science Letters*, 14: 1–13.

Rudnick, R.L., and Fountain, D.M., 1995. Nature and composition of the continental crust: a lower crustal perspective. *Reviews of Geophysics*, 33: 267–309.

Rudnick, R.L., and Gao, S., 2003. Composition of the continental crust. In: Rudnick, R.L., Holland, H.D., and Turekian, K.K. (eds.), *the Crust* (vol. 3). Treatise on the Geochemistry. Elsevier-Pergamon, Oxford, 1–64.

Sun, S.S., and McDonough, W.F., 1989. Chemical and isotopic systematics of oceanic basalts: implications for mantle composition and processes. In: Saunders, A.D., and Norry, M.J. (eds.), *Magmatism in the Ocean Basins*. Geological Society Special Publication, London, 313–345.

Turner, S., Arnaud, N., Liu, J., Rogers, N., Hawkesworth, C., Harris, N., Kelley, S., van Calsteren, P., and Deng, W., 1996. Post-collision, Shoshonitic volcanism on the Tibetan Plateau: Implications for Convective Thinning of the Lithosphere and the Source of Ocean Island Basalts. *Journal of Petrology*, 37: 45–71.

Wang Yang, 2007. *Mesozoic tectonic evolution of the Qiangtang Block: insights from geochronology, geochemistry and isotopes of volcanic rocks*. Master's thesis of the Graduate

School of the Chinese Academy of Sciences (in Chinese with English abstract).

Wang Yimin, Gao Yushu, Han Hhuiming and Wang Xiaohong, 2003. *Practical Handbook of Reference Materials for Geoanalysis*. Geological Publishing House (in Chinese).

Watson, E.B., and Harrison, T.M., 1983. Zircon saturation revisited: temperature and composition effects in a variety of crustal magma types. *Earth and Planetary Science Letters*, 64: 295–304.

Williams, H.M., Tumer, S.P., Pearce, J.A., Kelley, S.P., and Harris, N.B.W., 2004. Nature of the source regions for Post-collisional, Potassic magmatism in southern and northern Tibet from geochemical variations and inverse trace element modeling. *Journal of Petrology*, 45: 555–607.

Xu, R.H., Scharer, U., and Allegre, C.J., 1985. Magmatism and metamorphism in the Lhasa block (Tibet): a geochronological study. *Journal of Geology*, 93: 41–57.

Yin, A., and Harrison, T.M., 2000. Geology evolution of the Himalayan-Tibetan Orogen. *Annual Review of Earth and Planetary Science*, 28: 211–280.

Yin, J., Xu, J., Liu, C., and Li, H., 1988. The Tibetan plateau: regional stratigraphic context and previous work. Philosophical Transactions of The Royal Society A: Mathematical. *Physical and Engineering Sciences*, 327: 5–52.

Zhang, H.F., Sun, M., Lu, F.X., Zhou, X.H., Zhou, M., Liu, Y.S., and Zhang, G.H., 2001. Geochemical significance of a garnet Iherzolite from the Dahongshan kimberlite, Yangtze Craton, southern China. *Geochemistry Journal*, 35: 315–331.

Zhang, K.J., Cai, J.X., Zahgn, Y.X., and Zhao, T.P., 2006a. Eclogites from central Qiangtang, northern Tibet (China) and tectonic implications. *Earth and Planetary Science Letters*, 245: 722–729.

Zhang, K.J., Zhang, Y.X., Li, B., and Zhong, L.F., 2007. Nd isotopes of siliciclastic rocks from Tibet: constrraints on the pre-Cenozoic tectonic evolution. *Earth and Planetary Science Letters*, 256: 604–616.

Zhang, K.J., Zhang, Y.X., Li, B., Zhu, Y.T., and Wei, R.Z., 2006b. The blueschist-bearing Qiangtang metamorphic belt (northern Tibet, China) as an in situ suture zone: evidence from geochemical conmparison with the Jinsa suture. *Geology*, 34: 493–496.

Zhou Hua, Qiu Jiansheng, Yu Sibin and Wang Ruiqiang, 2016. Geochronology and geochemistry of volcanic rocks from Coqen district of Tibet and their implications for petrogenesis. *Acta Geologica Sinica*, 90(11): 3173–3191 (in Chinese with English abstract).

Zhu, D.C., Pan, G.T., Mo, X. X., Wang, L.Q., Zhao, Z.D., and Geng, Q.R., 2006. Identification for the Mesozoic OIB-type basalts in central Qinghai-Tibetan Plateau: Geochronology, geochemistry and their tectonic setting. *Acta Geologica Sinica* (English Edition), 80(6): 1312–1328.

About the first author

LIU Shen, male; born in 194 in Xi'an Sity, Shaanxi Province; PhD; graduated from Jilin Unviersity; professor of Northwest University. He is now interested in the study on the North China Craton and the Qinghai–Tibet plateau, lithospheric extension, destruction of the North China Craton and uplifting of the Qinghai-Tibet plateau. Email: liushen@vip.gyig.ac.cn; liushen@nwu.edu.cn.